

# Hyperion Validation Report

July 16, 2003

Jay S. Pearlman  
*Phantom Works*  
*The Boeing Company*  
*Kent, WA 98032*

**Boeing Report Number 03-ANCOS-001**

NASA/GSFC

## TABLE OF CONTENTS

1. BACKGROUND .....	1
2. INSTRUMENT OVERVIEW .....	2
3. INSTRUMENT CALIBRATION AND PERFORMANCE .....	6
3.1 Radiometric Calibration.....	6
3.2 Optical Calibration.....	14
3.3 Spectral Calibration .....	18
3.4 Polarization .....	26
4. IMAGE AND DATA PROCESSING .....	27
5. LESSONS LEARNED.....	30
6. CONTACT INFORMATION.....	30
7. SUMMARY .....	31
8. REFERENCES .....	31
APPENDIX A – HYPERION WAVELENGTHS .....	34

## LIST OF ILLUSTRATIONS

Figure 1. Hyperion has Three Units, the HEA (ul), CEA (II) and the HAS (right).....	2
Figure 2. The Pulse Tube Cryocooler Consists of a Cooler Unit, Control Electronics Box and an LVDT Box .....	3
Figure 3. The Hyperion Sensor Assembly Contains the Optical Systems, Cryocooler, In-flight Calibration System and High Speed Focal Plane Electronics .....	4
Figure 4. The Focal Plane Assemblies for the VNIR (a) and SWIR (b) Spectrometers.....	5
Figure 5. Hyperion Signal to Noise Performance .....	7
Figure 6. Comparison of Hyperion Synthesized Landsat-7 Data (left) and Landsat-7 ETM+ Data (right) Over the Same Location.....	10
Figure 7. Detailed Intensity Plot Across Both Images of Figure 6 .....	10
Figure 8. VNIR Spectrometer Repeatability Using Lunar and Solar Calibration. Values are Referenced to a Baseline of April 7, 2001 and 753 nm.....	11
Figure 9. SWIR Spectrometer Repeatability Using Lunar and Solar Calibration .....	11
Figure 10. The Hyperion SWIR “Echo” as Seen in the Moomba Gas Flare Scene, Before and After Echo Correction .....	12
Figure 11. The Echo Intensity Variation as Measured Across the Hyperion SWIR Focal Plane Array....	12
Figure 12. Lunar Images with Black Space Background (a) Show a Very Small Crosstalk (<1%) in the VNIR Output (b) .....	13
Figure 13. Noise Levels in the Four Quadrants of the VNIR FPA. Quadrants C and D had More Noise and D Showed Pattern Noise. ....	14
Figure 14. Knife-edge Measurements and Analysis Provide MTF Characteristics .....	15
Figure 15. Two Dimensional Patterns Were Used to Measure MTF.....	16
Figure 16. The Mid-Bay Bridge Near Eglin AFB in Destin, FL, was Used to Measure the MTF .....	17
Figure 17. On-orbit Measurements of MTF Using Interlaced Bridge Images.....	17
Figure 18. VNIR Spectral Variation Across the Field of View .....	20
Figure 19. SWIR Spectral Variation Across the Field of View.....	20
Figure 20. SWIR Portion of the Internal Calibration Image Displaying Instrument Covet Paint Spectral Patterns.....	21
Figure 21. Reflectance Spectra of Doped Spectralon .....	22
Figure 22. Comparison of High Resolution and Hyperion Measurement of Erbium-doped Spectralon ...	22
Figure 23. Measurement of Hyperion Spectral Response Before (TRW) and After Spacecraft Integration and Environmental Testing (GSFC).....	23
Figure 24. Atmospheric Limb Measurements Enable Spectral Measurement Without Earth Background.....	24
Figure 25. Six Spectral Profiles of the Atmospheric Limb, Measured at Different Grazing Positions ....	24
Figure 26. Analysis of Atmospheric Limb Measurement Showing: Hyperion Spectra of Atmospheric Limb Collect (red); Measured Diffuse Cover Reflectance (blue); and Atmospheric Reference Profile from Modtran 3 (black) .....	25
Figure 27. Comparison of Laboratory and On-orbit Smile Characteristics for Spectral Channels 17 and 41 .....	25
Figure 28. Differences in Laboratory and On-orbit Spectral Calibrations for the VNIR (left) and SWIR (right) Spectrometers .....	26
Figure 29. VNIR and SWIR Polarization Characteristics.....	27
Figure 30. Dark Signal Drift as a Function of Time During a Data Collection Sequence.....	28
Figure 31. Sample Spectra From Level 1 Processing .....	29

## LIST OF TABLES

Table 1. Characteristics of the Hyperion System Hyperion Instrument .....	6
Table 2. On-orbit Performance of the Hyperion Instrument.....	6
Table 3. Tradeoffs of Approached to On-orbit Radiometric Calibration.....	8
Table 4. MTF Lab Measurement Results Using Knife-edge Technique .....	15
Table 5. Measurement of GSD Over Many Images Show Good Consistency .....	18
Table 6. Hyperion Spectral Calibration Derived from Laboratory Monochrometer Measurements .....	19
Table 7. Evolution of Level 1 Processing .....	28

## **ABSTRACT**

The Hyperion Instrument was the first imaging spectrometer to routinely acquire science grade data from earth orbit. As part of the NASA New Millennium Program Earth Observing – 1 Mission, the focus of the program was on instrument performance validation and application assessments. Innovative techniques for spectral calibration of space-based sensors were also tested and validated. Instrument performance met or exceeded predictions including continued operation well beyond the planned one-year program. This document presents the instrument design approach, performance and lessons learned from the Hyperion program. This document addresses the first year of mission and instrument operations.

# 1. BACKGROUND

The NASA New Millennium Program (NMP) was created to flight-validate instrument and spacecraft technologies that may enable new or more cost-effective approaches to Earth observation [1]. Both advanced multispectral imagers and hyperspectral imagers were part of the NMP Earth Observing-1 mission. Originally, these two classes of instruments were to be integrated into a single design using a common set of fore-optics. However, in the interests of flexibility and time, a parallel development path was chosen and the multispectral Advanced Land Imager (ALI) and the hyperspectral Hyperion became separate instruments. The Hyperion instrument was built by TRW, Inc. (now Northrop Grumman Space Technology) with strong support from key sensor subsystem organizations [2]. The Hyperion project had a fast-track schedule and was delivered to NASA Goddard Space Flight Center (GSFC) for spacecraft integration in less than 12 months. To accomplish this, TRW used focal planes and associated electronics remaining from the NASA Lewis Small Satellite Technology Initiative (SSTI) hyperspectral mission.

As an important demonstration instrument, emphasis was placed on quality characterization and calibration. For pre-launch radiometric measurements, National Institute of Standards and Technology (NIST)-traceable lamps and solid-state detectors were used for radiometric measurements. Teams from MIT/Lincoln Laboratory, NASA GSFC and the Jet Propulsion Laboratory (JPL) participated in the radiometric calibration. Each of these groups brought sources or transfer standards to TRW during the laboratory environmental testing. The results of these measurements were ultimately integrated into the on-orbit calibration.

The instrument's end-to-end testing included an image simulator that allowed creation of two-dimensional spatial images for both instrument characterization and for testing the image processing system. The image processing software was developed by TRW and the Level 0 processing code, from raw data to an uncalibrated imageable format, was delivered to NASA GSFC for production operations. The data were processed to radiometrically calibrated Level 1 format at TRW during the first year of operations. In later years of the mission, the processing was done at the U. S. Geological Survey (EROS Data Center).

Following launch, the on-orbit characterization lasted for 120 days [3] with continuing assessment of the instrument throughout the first year of operations. Much of the laboratory calibration carried through to the on-orbit operations. Several areas, however, are worth noting. For example, following launch, there was as much as a 30% change in the on-board calibration lamp output, which was ascribed to a change in lamp characteristics due to operation in zero gravity.

The instrument was very stable and variations in calibration of 1% in the VNIR and 3% in the SWIR were measured during the first year of operation using lunar observation data. After one year of operations, the radiometric coefficients were modified to combine the vicarious, lunar, solar and updated laboratory calibrations. The visible-near infrared (VNIR) and short-wave infrared (SWIR) spectrometer gains were increased 8% and 18% respectively. This was a recalibration rather than a change in the instrument performance.

Hyperion was designed for a one-year life. The instrument has continued to function well beyond two years with no degradation. Details of the instrument design, performance and data processing are provided in the following sections.

## 2. INSTRUMENT OVERVIEW

The Hyperion pushbroom instrument was designed to provide high quality calibrated data for hyperspectral application evaluations [4]. With Hyperion, each pushbroom image frame captured the spectra from an area 30 m along-track by 7.7 km cross-track. The forward motion of the satellite created a sequence of frames that were combined into a two-dimensional spatial image with a third dimension of spectral information (called a “3-d data cube”).

The pushbroom technology introduced new operations and performance characteristics in comparison to the traditional scanning sensors. Scanning instruments such as the Landsat 7 ETM+ used linear detector arrays and a mirror that scans in the cross track direction in order to create multi-band, two-dimensional images. As array technology improved, two dimensional focal plane arrays became available for space-based remote sensing. The advantages of using 2-D arrays were that they generated a two dimensional, spectral image without the need for moving parts and they had longer dwell times, giving increases in signal to noise performance. The challenges of a pushbroom configuration were that a multitude of pixels needed to be calibrated and the natural calibration process in the scanning system was not available – i.e., the scanning mirror allowed a calibration source to be routinely swept across the detectors, providing continuous calibration. Addressing these challenges was a key facet of the Hyperion program.

Hyperion had a single telescope and two spectrometers: one visible/near infrared (VNIR) spectrometer and one short-wave infrared (SWIR) spectrometer. The Hyperion instrument consisted of three physical units: (1) the Hyperion Electronics Assembly (HEA); (2) the Cryocooler Electronics Assembly (CEA); and (3) the Hyperion Sensor Assembly (HSA) (Figure 1). These units were placed on the nadir deck of the spacecraft with the viewing direction along the major axes of the spacecraft.

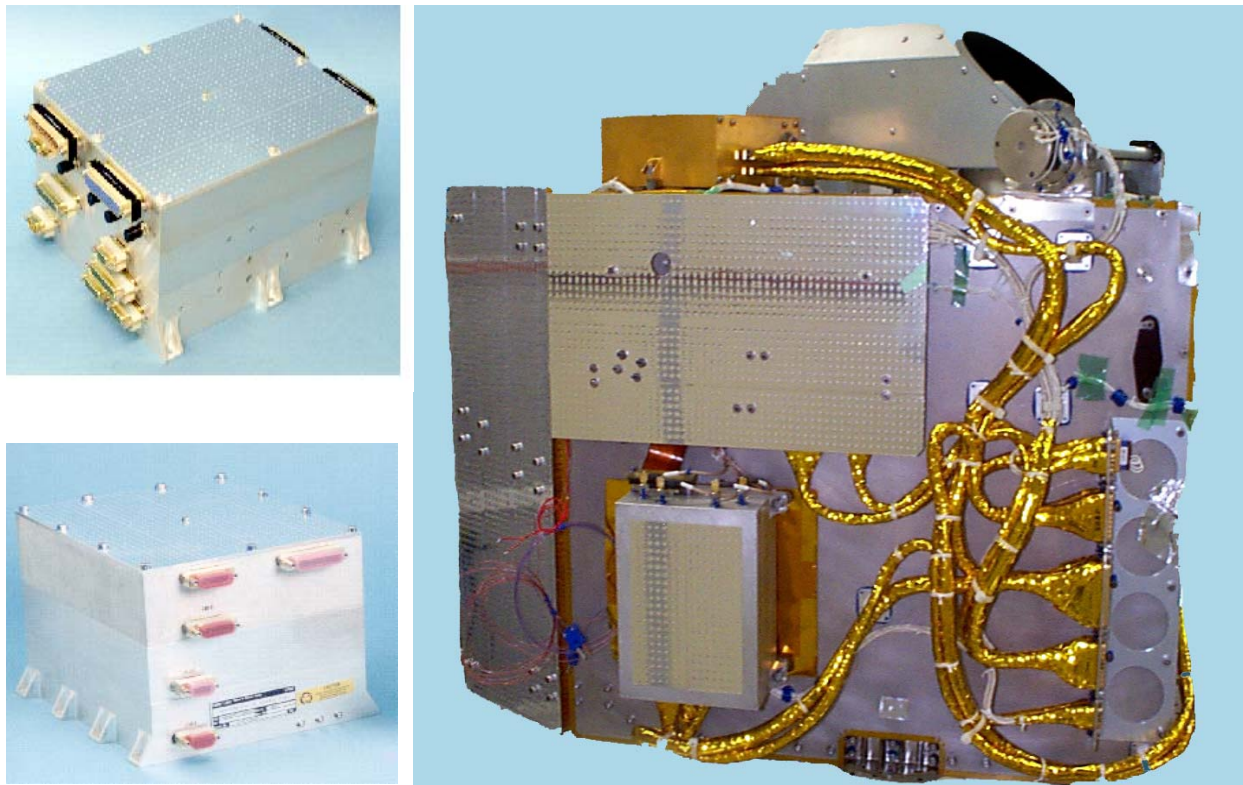


**Figure 1. Hyperion has Three Units, the HEA (ul), CEA (ll) and the HAS (right)**

The HEA contained the interface and control electronics for the instrument. It consisted of electronics to: (1) convert spacecraft 28VDC power to instrument power; (2) support spacecraft command and telemetry via a 1773 data bus; (3) collect and digitize the instrument state of health data; (4) collect and digitize the VNIR and SWIR science data from the corresponding analog signal processors; (5) support science data transmission to the spacecraft over two 32-wire RS-422 data buses; and (6) support command and telemetry functions for the CEA.

The Cryocooler Electronics Assembly (CEA) controlled the cryocooler operations and consisted of electronics to: (1) convert spacecraft 28VDC power to cryocooler power; (2) support spacecraft command and telemetry via the HEA using an RS-422 data bus; and (3) collect performance data from the pulse tube cooler and provide feedback control for optimal operation of the cryocooler. The cryocooler design was selected because its low vibration minimized movements near the focal plane. The cryocooler system is shown in Figure 2. The cooler was connected to the focal plane array via a cold thermal strap. It provided an estimated 0.84 W of cooling while consuming 14.7 W of electrical power. Typically, it operated with a 79% margin. Details of the cooler and its operation are given in Reference [5].

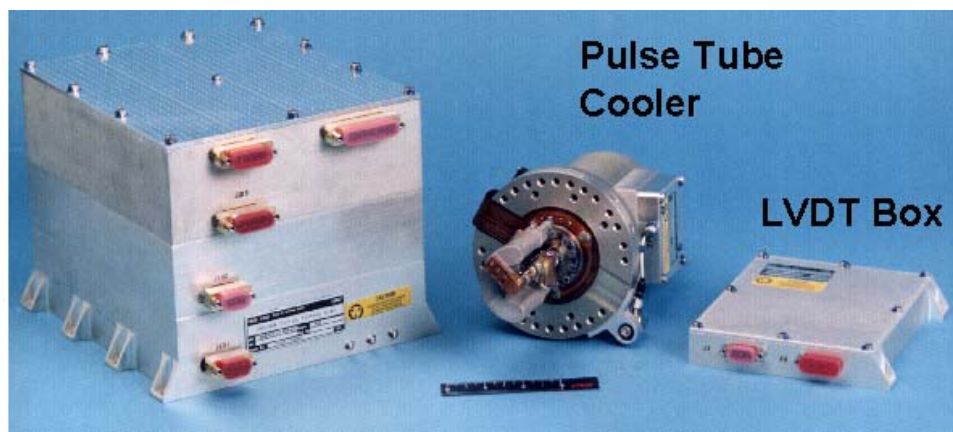


**Figure 2. The Pulse Tube Cryocooler Consists of a Cooler Unit, Control Electronics Box and an LVDT Box**

The HSA included the optical systems, cryocooler, in-flight calibration system and the high-speed focal plane electronics (Figure 3). The HSA enclosure was 38.6 cm wide, 75 cm long and 64.6 cm high. The HSA enclosure controlled the optics thermal environment and the housing was maintained at  $20^{\circ} \pm 2^{\circ}\text{C}$  for precision imaging and alignment. The VNIR spectrometer focal plane array (FPA) (see Figure 4) was passively cooled by a radiator and operated at  $10^{\circ}\text{C}$ . The SWIR spectrometer FPA was actively cooled by the cryocooler with a thermal head set to 110 K.

The Hyperion telescope (fore-optics) was a three-mirror astigmat design with a 12 cm primary aperture and an effective f-number of 11. The telescope imaged the Earth onto a slit that defined the instantaneous 0.624 degrees wide field-of-view (i.e., 7.7 km swath width from a 705 km altitude) by  $42.55 \mu$  radians (30 meters) in the satellite velocity (along track) direction. This slit image of the Earth was relayed at a magnification of 1.38:1 to two focal planes, one in each of the two grating imaging spectrometers. A dichroic filter in the system reflected the band from 400 to 1,000 nm to the VNIR spectrometer and transmitted the band from 900 to 2,500 nm to the SWIR spectrometer. The SWIR overlap with the VNIR from 900 to 1000 nm allowed a couple of bands for cross calibration of the two spectrometers. Both spectrometers used JPL convex gratings [6] in a 3-reflector Offner configuration. There was an order-sorting filter in the VNIR spectrometer.

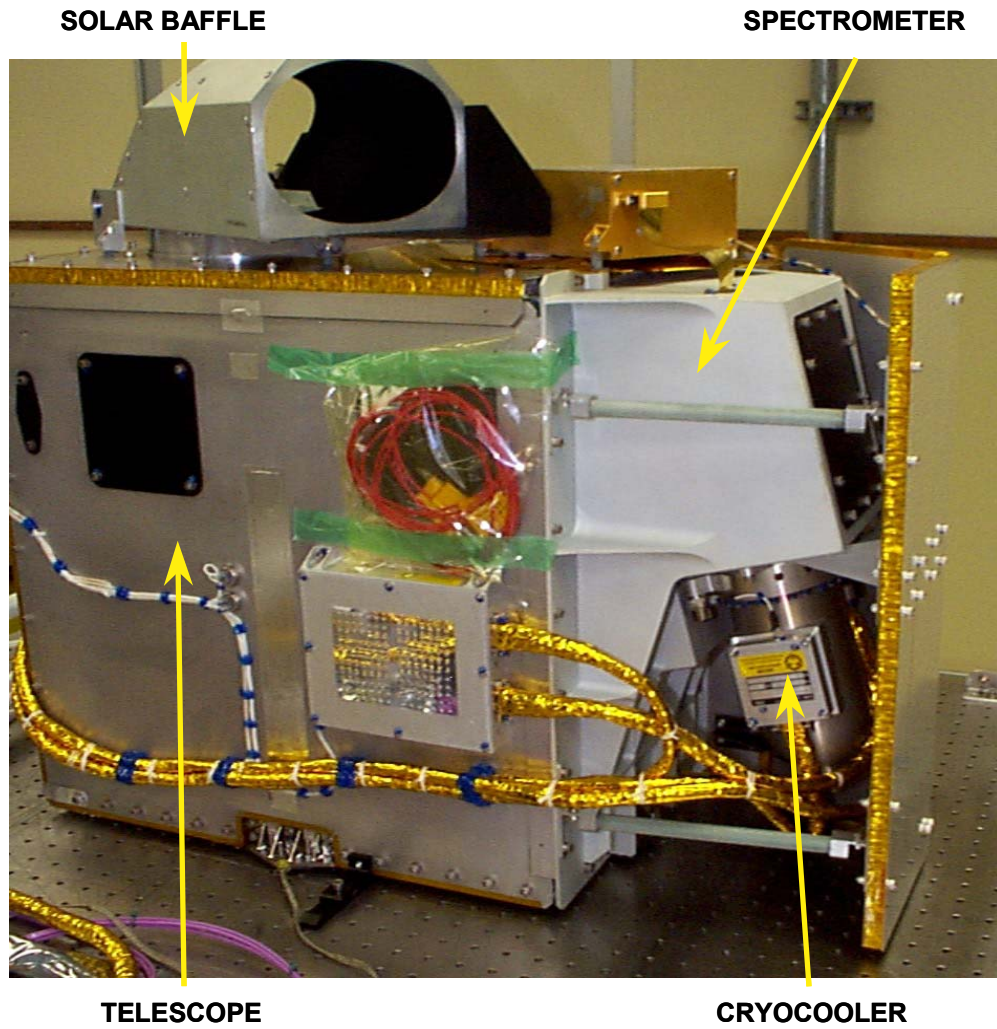


**Figure 3. The Hyperion Sensor Assembly Contains the Optical Systems, Cryocooler, In-flight Calibration System and High Speed Focal Plane Electronics**

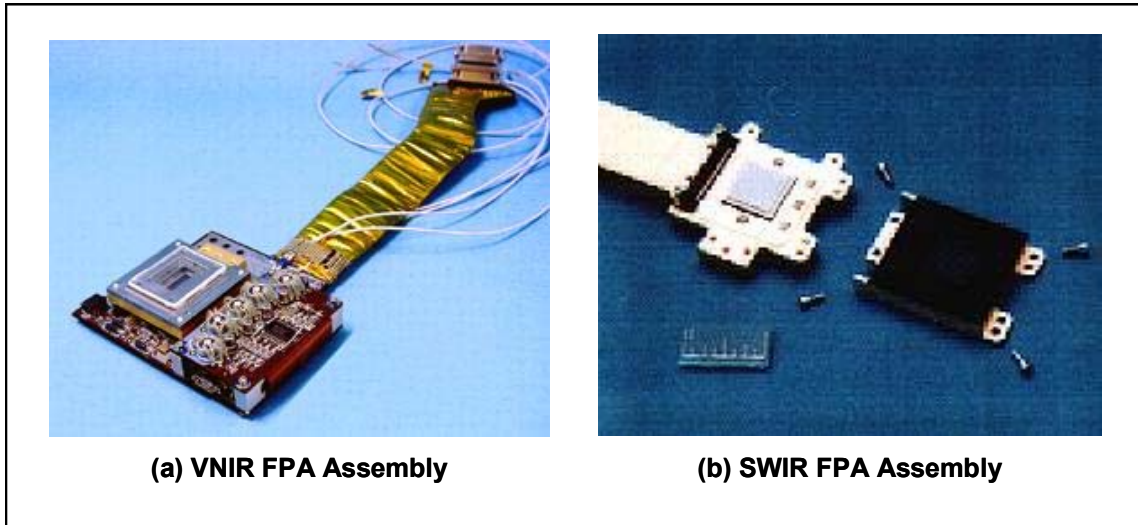


**Figure 4. The Focal Plane Assemblies for the VNIR (a) and SWIR (b) Spectrometers**

The motorized HSA cover was an integral part of the instrument calibration process; the cover had three positions: open, closed and calibration. The backside of the aperture cover was coated with a diffuse reflecting white, silicone thermal control paint. With the aperture cover in calibration position (partially open at 37 degrees), solar illumination reflecting off the diffuse painted surface was used as a source for the on-orbit radiometric calibration. With the cover closed, the internal calibration lamps reflected off the painted cover. For these two calibration techniques, the paint was characterized for reflectivity as a function of angle [7].

The VNIR spectrometer used a 70 (spectral) x 256 (spatial) pixel section of the 128 x 256 silicon FPA. The Mercury Cadmium Telluride (HgCdTe) SWIR FPA had 256 x 256 pixels of 60  $\mu\text{m}$  pitch and a custom pixel readout. For Hyperion, only a 172 pixel (spectral) x 256 pixel (spatial) section of the FPA was used. While the total number of bands was 242, signal-to-noise considerations led to only 198 pixels being routinely processed by the Level 1B software (see Section 4). Originally, the design was to use 250 pixels cross-track, leaving a six pixel buffer for VNIR/SWIR alignment. However, on-orbit testing showed that the two spectrometers were aligned to one pixel cross track offset and, as a result, all 256 cross track pixels were collected and processed.

During the instrument design, a number of tradeoffs were made to increase the signal-to-noise for an orbit of 705 km altitude. Hyperion was built using existing focal planes designed for operation at a 520 km altitude orbit. Orbiting at the higher 705 km orbit reduced the signal-to-noise by almost a factor of two. To counter this, the original Lewis instrument bandwidth of 5 nm was increased to 10 nm for Hyperion. For the same reason, two spectrometers with JPL curved gratings were used rather than a single spectrometer with a dual-blazed grating.

The general instrument characteristics are given in Table 1. A summary of the on-orbit performance is given in Table 2. Details of the characterization and performance are provided in the next section.

**Table 1. Characteristics of the Hyperion System**

Parameter	Hyperion
Volume (L x W x H, cm)	39 x 75 x 66
Mass (kg)	49
Average Power (W)	51
Aperture (cm)	12
IFOV (mrad)	0.043
Crosstrack FOV (deg)	0.63
Wavelength Range (nm)	400 – 2500
Spectral Resolution (nm)	10
Number of Spectral Bands	220
Digitization	12
Frame Rate (Hz)	223.4

**Table 2. On-orbit Performance of the Hyperion Instrument**

	Characteristic	On-orbit
<b>OPTICAL</b>	<b>GSD (m)</b>	<b>30.38</b>
	<b>Swath (km)</b>	<b>7.6</b>
	<b>VNIR MTF @ 630nm</b>	<b>0.23-0.27</b>
	<b>SWIR MTF @ 1650nm</b>	<b>0.28</b>
	<b>Spatial Co-Reg: VNIR</b>	<b>.18 @ Pix #126</b>
<b>RADIO-METRIC</b>	<b>Spatial Co-Reg: SWIR</b>	<b>.21 @ Pix #131</b>
	<b>Abs. Radiometry (1Sigma)</b>	<b>3.40%</b>
	<b>VNIR SNR (550-700nm)</b>	<b>140-190</b>
	<b>SWIR SNR (~1225nm)</b>	<b>96</b>
	<b>SWIR SNR (~2125nm)</b>	<b>38</b>
<b>SPECTRAL</b>	<b>No. of Spectral Channels</b>	<b>198 Processed</b>
	<b>VNIR (bands 8-57)</b>	<b>427-925 nm</b>
	<b>VNIR Bandwidth (nm)</b>	<b>10.19-10.21</b>
	<b>VNIR X-trk Spec. Error</b>	<b>2.2 nm</b>
	<b>SWIR (bands 77-224)</b>	<b>912 - 2395 nm</b>
	<b>SWIR Bandwidth (nm)</b>	<b>10.08-10.09</b>
	<b>SWIR X-trk Spec. Error</b>	<b>0.58 nm</b>

### 3. INSTRUMENT CALIBRATION AND PERFORMANCE

#### 3.1 Radiometric Calibration

The use of a two-dimensional focal plane pushbroom configuration versus a more traditional side-scanned linear array required new approaches to calibration.

##### 3.1.1 Pre-Launch Calibration

For the pre-launch calibration, TRW used its MultiSpectral Test Bed (MSTB)[8]. The MSTB consisted of a monochromator whose output was in one of two optical configurations: either (1) the monochromator light illuminated a pinhole, slit or knife edge which was at the focus of an off-axis parabola reflector; or (2) the monochromator light illuminated a spectralon panel whose reflection was collimated by the same off-axis parabola. Absolute radiometric standards and NIST traceable sources/detectors were used for the characterization. Typically, the light from the MTSB was directed onto the transfer radiometer or into the Hyperion aperture and the two measurements were compared using the same light source. The data were then analyzed and the absolute reference was transferred to Hyperion to determine the radiometric gain coefficients.

Pre-launch calibration laboratory observations used both lamp-based and solid-state detector measurements [7], including the GSFC Landsat Transfer Standard [9] for cross calibration with the EO-1 Advanced Land Imager (ALI) instrument. For Hyperion, the lamp-based (including the Landsat Transfer Standard and the JPL measurements) and solid-state detector-based calibrations showed a 5-15% difference in absolute values but similar spectral response profiles. The solid-state detectors values were used for the pre-launch baseline. Based on the measured performance, the signal-to-noise performance was calculated (Figure 5). The baseline conditions assumed for the performance model are a solar zenith angle of 60 degrees, a 30% uniform albedo, an instrument with f/11 optics, a 10 nm bandwidth, and a 224 Hz frame rate. These were very conservative because other instruments typically use a 50% albedo and a solar zenith angle of less than 45 degrees.

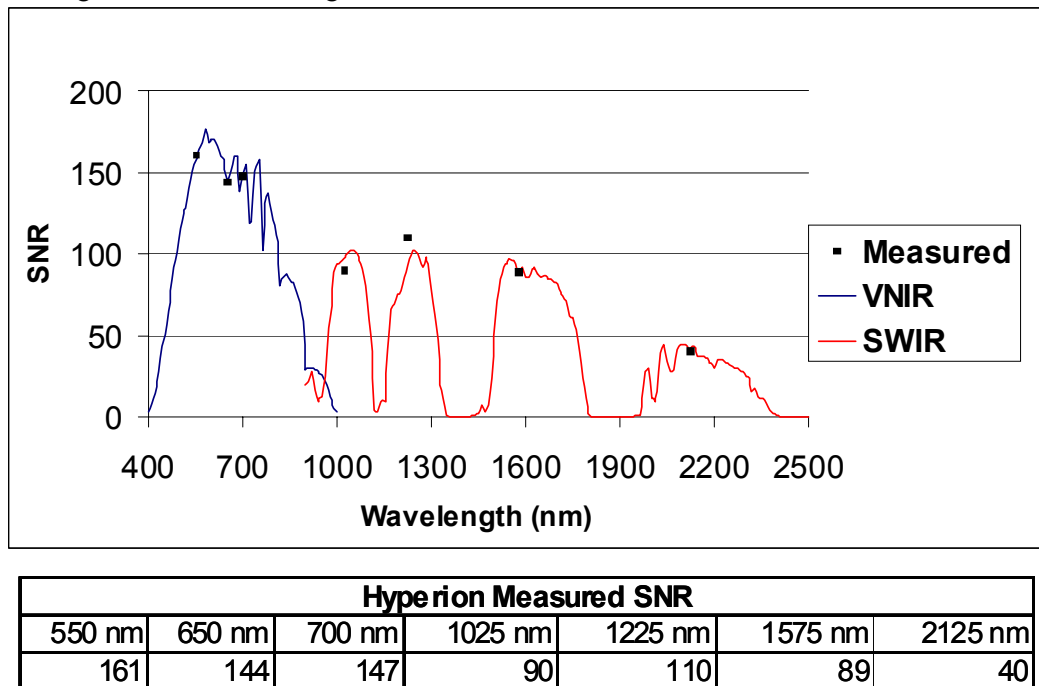


**Figure 5. Hyperion Signal to Noise Performance**

Another factor that impacted the radiometric calibration was ice accumulation on the SWIR FPA. This was first observed after integration of Hyperion onto the spacecraft at GSFC. Recycling of the SWIR temperature to room temperature and back removed the effect and the original baseline performance of the instrument was again achieved. Since there did not appear to be any residual degradation, it was hypothesized that the cause of the contamination was freezing of water vapor onto the focal plane. The cause of the water vapor contamination was never determined. The ice accumulation was also observed on-orbit and was predictable enough that the cryocooler recycling was scheduled more than a week in advance. This avoided the loss of priority data.

### 3.1.2 On-Orbit Radiometric Calibrations

Solar, lunar and earth-surface-observing “vicarious” measurements were used for the on-orbit calibration. Pointing agility of the EO-1 satellite enabled unique calibration experiments (in addition to traditional solar and vicarious measurements) to help quantitatively analyze instrument performance including active illumination experiments and lunar (radiometric), atmospheric limb (spectral) and 90 degree yaw (slit in-track) (uniformity) observations. All of these measurements had strengths and weaknesses (Table 3).

**Table 3. Tradeoffs of Approached to On-orbit Radiometric Calibration**

<u>Technique</u>	<u>Pro</u>	<u>Con</u>
Solar	<ul style="list-style-type: none"> <li>•Stable source</li> <li>•Uniform illumination</li> </ul>	<ul style="list-style-type: none"> <li>•Diffuser reflection may change</li> </ul>
Lunar	<ul style="list-style-type: none"> <li>•Direct view of source</li> </ul>	<ul style="list-style-type: none"> <li>•Infrequent access</li> <li>•Requires special maneuvers</li> <li>•Uncertainty of lunar model</li> </ul>
On-board lamps	<ul style="list-style-type: none"> <li>•Routinely available</li> </ul>	<ul style="list-style-type: none"> <li>•Uncertain long term stability</li> <li>•Diffuser may change</li> </ul>
Vicarious Earth observations	<ul style="list-style-type: none"> <li>•Direct view of source</li> <li>•Cross ref to ground cal</li> </ul>	<ul style="list-style-type: none"> <li>•Atmospheric impacts</li> <li>•Cost</li> </ul>

#### Solar Calibration

For solar calibration, the sunlight was reflected from diffuse paint deposited on the rear of the instrument cover. The solar calibration was unique in that it provided a uniform cross-track reference with a very stable source. It was conducted about once per week during the first year of operations for both absolute calibration and to initially update the pre-flight calibration files by correcting for pixel-to-pixel variations [10]. While the sun is stable, there was the potential for long-term temporal variations in the diffuser characteristics that could potentially lead to a drift in calibration. There was also some small uncertainty due to variations in spacecraft pointing. The solar calibration was done by pointing Hyperion so that the solar baffle was aligned offset from the spacecraft-sun axis. The spacecraft was yawed to transition the solar baffle and instrument observation axis across the sun. This eliminated the need to point directly at the sun early in the mission. Since this was a new spacecraft, some uncertainty in the spacecraft pointing was expected. The yaw motion only addressed one axis. To ensure that the pointing was correct on both axes, early in the mission, the spacecraft was maneuvered so that the sun angle varied over  $\pm 6$  degrees about the spacecraft-sun axis to induce vignetting of the solar radiation by the solar baffle. The correct pointing orientation was then established to avoid subsequent vignetting.

#### Lunar Calibration

Lunar calibration did not use a diffuser, as the instrument views the moon directly and with no intervening atmosphere. These benefits were balanced by the need for special spacecraft maneuvers and by the uncertainties of the lunar reflection model. Lunar observations were conducted near a 7 degrees lunar phase angle each month since January 2001[11]. For each lunar observation, the spacecraft was maneuvered to scan the Moon in the in-track direction at 1/8 of the nominal scan rate in order to over-sample the lunar disk. The lunar spectral irradiance was obtained by summing the calibrated lunar image. Once the measured lunar irradiance was calculated for a given observation, the expected lunar irradiance

for the time of the observation was calculated by the U. S. Geological Survey using data obtained from the RObotic Lunar Observatory (ROLO) in Flagstaff Arizona [12]. Since 1996, ROLO has been measuring the lunar irradiance between 350 and 2500 nm as a function of phase angle as often as weather and visibility permit [13].

A model of the lunar irradiance was required and depended on the spacecraft position, as well as the relative positions of the earth, moon and sun [14]. The absolute radiometric scale of the lunar model was based on standard stars [15] and although the absolute scale was in general agreement with several spacecraft [16], the uncertainty was not well understood. Direct calibration of the ROLO system traceable to the NIST is underway.

### Internal Lamp Calibration

Testing of the internal calibration lamps was done to weed out infant mortality [17]. There was a lamp failure during the thermal-vacuum testing at TRW. A post-mortem and extensive analysis in collaboration with NASA GSFC did not resolve the cause. The lamp string was rebuilt and provided satisfactory operations during the remainder of the ground testing. Despite this, just prior to launch, one of the redundant lamp strings failed. This eliminated the option of intensity steps for linearity response measurements. Since the launch was imminent, it was decided to fly with only one lamp string. On-orbit radiometric calibration was performed with the remaining lamps.

Initially, the lamps were designed as a radiometric transfer standard between pre-flight and on-orbit calibrations. However, a large increase in lamp output of 30% or more was seen in the VNIR and SWIR immediately after launch. This was attributed to a loss of convective cooling of the filament in the zero-G environment and invalidated using the reference lamps as calibration transfer standards between preflight and flight calibration [17]. As experience was gained with solar and lunar calibrations showing the stability of the instrument was better than 3% long term, the lamps played a smaller role in calibration and characterization. By six months after launch, the lamps were not routinely included in the Level 1 processing.

### Vicarious Calibration

Vicarious calibration involved imaging a characterized test area on the earth's surface. Vicarious calibration was an important factor in the instrument characterization program because the scene was viewed directly rather than off a diffuser. Vicarious calibration also facilitated comparison with Landsat 7 and other space-based imaging systems [18]. A broader range of inter-comparisons such as solar and lunar imaging would have been beneficial, but were not within the modes of other operational imagers. For the calibration, ground truth and atmospheric characterization were performed with ground-based instruments. These measurements were projected to radiances at the spacecraft through an atmospheric model. The challenges were in extrapolating a surface point measurement to a pixel area in the image and in correcting for atmospheric effects. Sites for vicarious calibration were selected in both the northern and southern hemispheres to allow measurements with a high sun angle throughout the year. Sites included Lake Frome in South Australia, Arizaro in Argentina, Railroad Valley in the United States and others. These areas were dry lake beds and salt flats with generally high reflectivity. Lake Frome [19] had 60% reflectivity in the VNIR spectrum. Arizaro had both high reflectivity and was at very high altitude (>4000 m) [20], reducing the impact of the atmosphere, but making the atmospheric modeling more difficult. Railroad Valley is a well-characterized site with easy access to permit frequent measurements [21].

The challenge with vicarious calibration for a pushbroom system was finding sites uniform enough in the cross track direction so that a large number of pixels can be tested under similar measurement conditions. This was generally not a significant issue with side-scanned systems such as Landsat 7. For the 7.7 km

swath of Hyperion, areas such as ice sheets in Greenland [22] were used. However, for large swath systems with 10's or 100's of kilometer cross-track visibility, other approaches need to be developed. One such concept was a Data Collection Event (DCE) in which the spacecraft is yawed ninety degrees so that the spectrometer entrance slit is aligned with the satellite velocity vector (rather than the nominal cross-track direction). In this configuration, each cross-track pixel passes over the same ground position within a short time. This promising technique is presently being evaluated. [23]

Ground sites were also used for a cross-calibration with Landsat 7. For this comparison, the Hyperion spectral bands were aggregated into the larger Landsat bands and a number of nearly simultaneous images over mineral and agricultural areas. With the current Hyperion calibration, the agreement between the two instruments was excellent, that is, within a few percent [18]. A comparison over the Coleambally Irrigation area is shown in Figures 6 and 7.

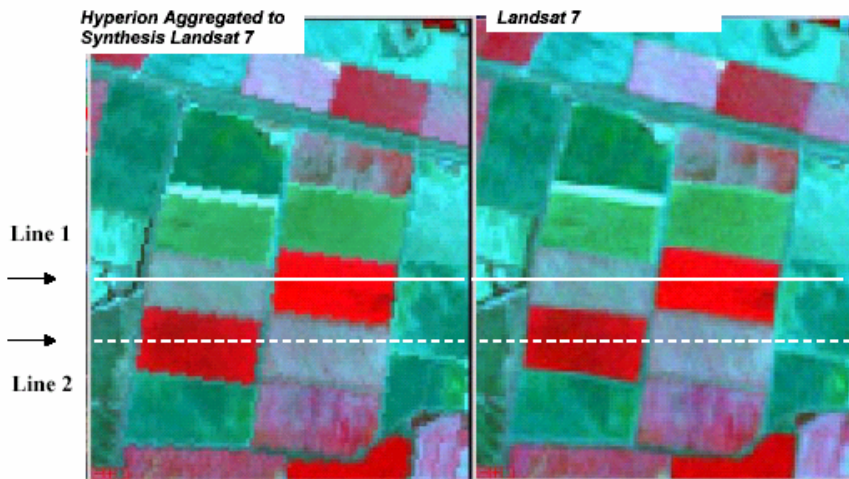


**Figure 6. Comparison of Hyperion Synthesized Landsat-7 Data (left) and Landsat-7 ETM+ Data (right) Over the Same Location**

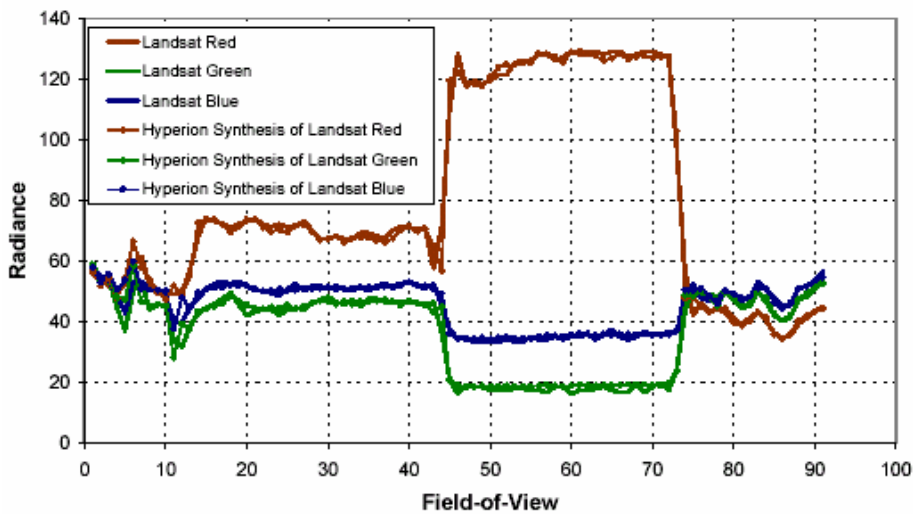


**Figure 7. Detailed Intensity Plot Across Both Images of Figure 6**

The radiometry of Hyperion was very stable. Data from a series of lunar and solar calibration collects used to monitor the continued repeatability of the VNIR and SWIR are shown in Figures 8 and 9. For this period, the VNIR repeatability is better than 1% and the repeatability of the SWIR is better than 3%. At the end of the first year, based on the full range of on-orbit radiometric measurements, a decision was made by TRW and the Science Validation Team (SVT) calibration team to increase the VNIR calibration coefficients by 8% and the SWIR by 18%. This brought the absolute radiometry into close agreement with vicarious and Landsat 7 results. The Level 1 data products using these revised factors were denoted Level 1B1.

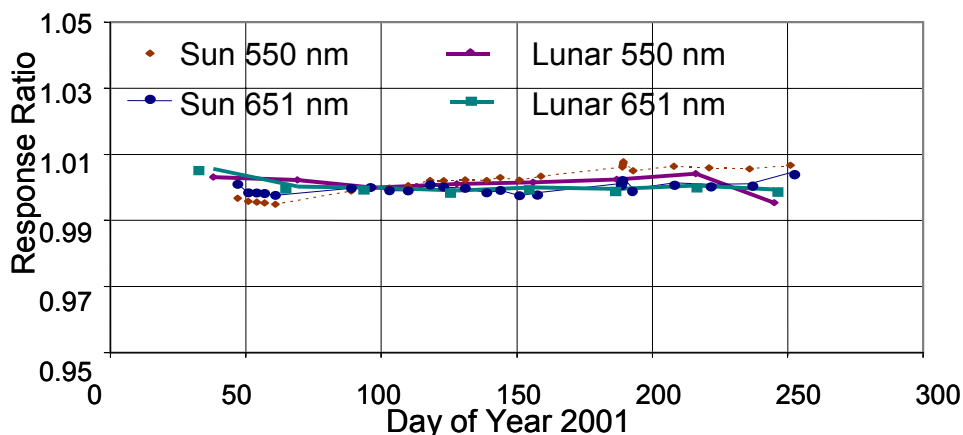


**Figure 8. VNIR Spectrometer Repeatability Using Lunar and Solar Calibration. Values are Referenced to a Baseline of April 7, 2001 and 753 nm.**

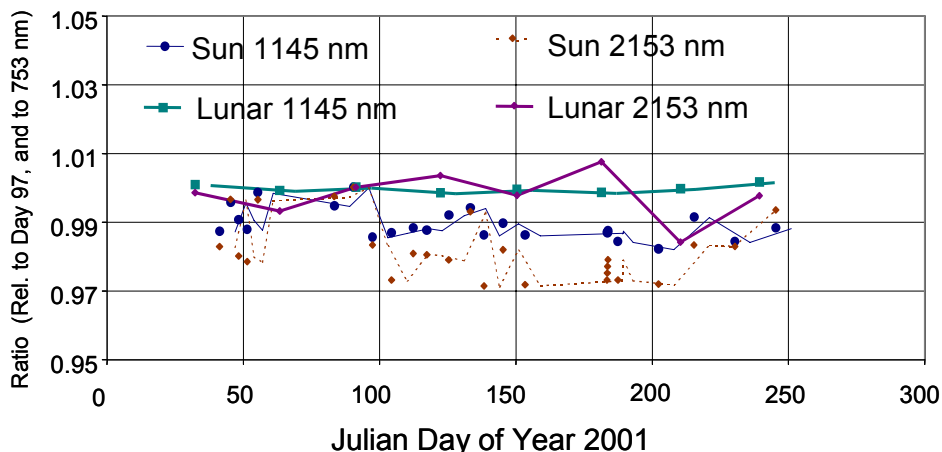


**Figure 9. SWIR Spectrometer Repeatability Using Lunar and Solar Calibration**

### 3.1.3 Other Radiometric Effects

In addition to the absolute calibration, certain features were observed during the prelaunch calibration that were characterized and then largely removed as part of the image processing to radiometrically corrected Level 1 data. These included both a SWIR “echo” and a SWIR “smear”. The echo resulted from electronic “cross-talk” in the SWIR spectrometer that caused a small anomalous signal to appear 11 lines offset in track. The effect is illustrated in Figure 10, which was the image of a very bright gas flare in Moomba, Australia. The magnitude of the echo was mapped for the entire focal plane and is typically

6.5%. The mapping and intensity profile of the echo from laboratory measurements are exhibited in Figure 11. The effect was stable and was readily removed as part of the Level 1 data processing.

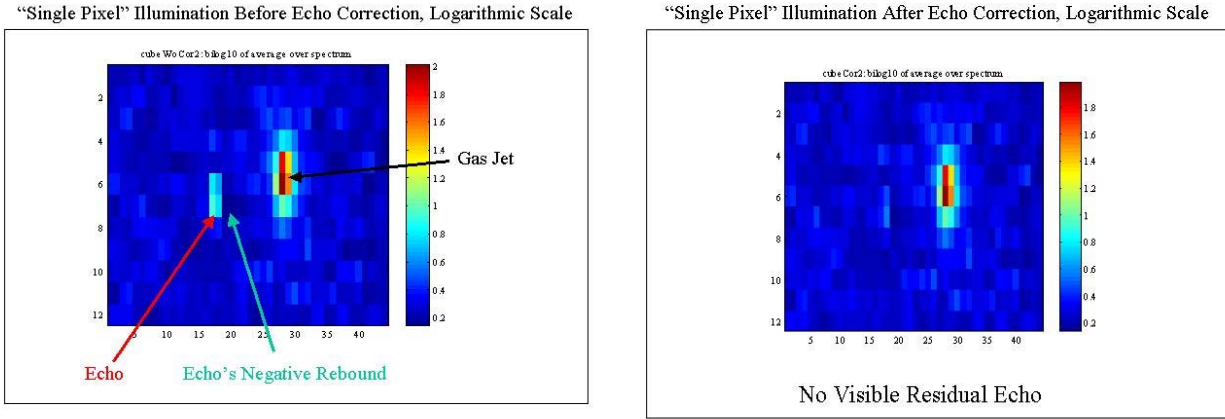


**Figure 10. The Hyperion SWIR “Echo” as Seen in the Moomba Gas Flare Scene, Before and After Echo Correction**

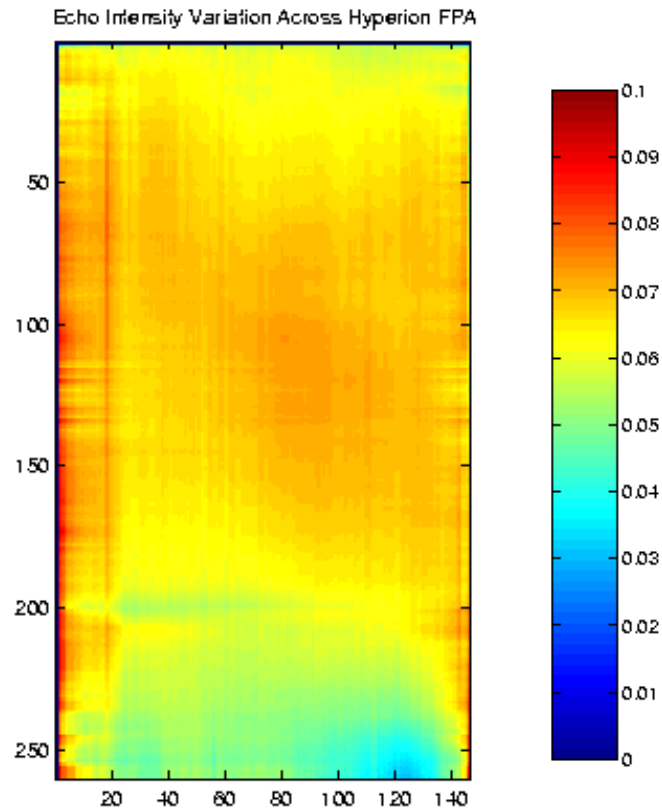


**Figure 11. The Echo Intensity Variation as Measured Across the Hyperion SWIR Focal Plane Array**

The SWIR smear was a local effect in which a small percentage of the signal from an adjacent pixel occurred in the pixel readout. This was due to incomplete charge transfer in the readout process. The value was approximately 6% and was repeatable. The effect was also removed during Level 1 processing.

Similar artifacts were observed with the VNIR spectrometer but to a much smaller extent. The maximum observed crosstalk was 0.9% with more typical levels of 0.5% for low-contrast scenes. The effect was observed most prominently with lunar images where there was very high contrast between lunar intensity and the blackness of deep space (see Figure 12).

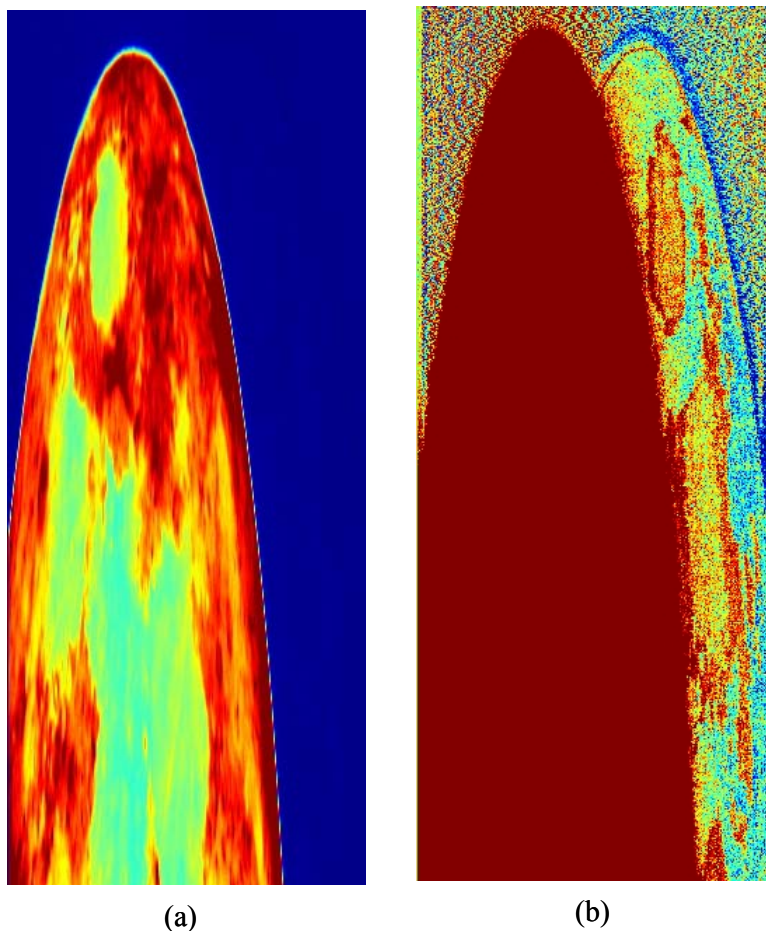


**Figure 12. Lunar Images with Black Space Background (a) Show a Very Small Crosstalk (<1%) in the VNIR Output (b)**

The VNIR readout electronics also contributed to the noise. The VNIR spectrometer had four readout quadrants, each of which had a slightly different noise level and pattern (Figure 13). In addition to random noise, a temperature dependent pattern in the dark images was seen in Quadrant D and was referred to as the “Dark Pattern”. While it was not consistent between data collections, the noise was stable within a DCE. Thus, the dark subtraction on a pixel-by-pixel basis removed the pattern from the Level 1 data.

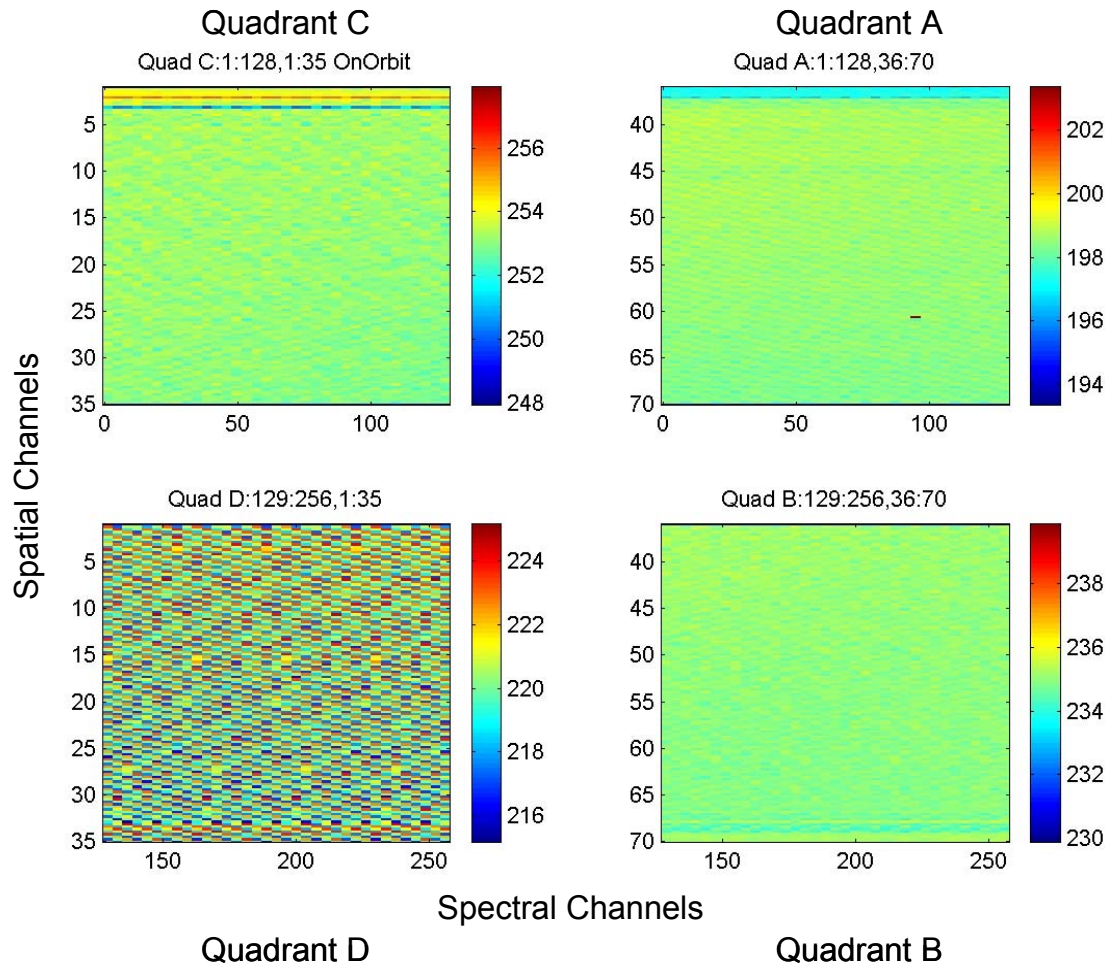


**Figure 13. Noise Levels in the Four Quadrants of the VNIR FPA. Quadrants C and D had More Noise and D Showed Pattern Noise.**

### 3.2 Optical Calibration

The optical performance of Hyperion was characterized by the modulation transfer function (MTF), the ground sample distance (GSD) and other parameters. In some cases, direct measurements were possible. In other cases, a combination of measurements and modeling was used.

#### Modulation Transfer Function (MTF)

In the laboratory, knife edges/slits and two-dimensional patterns were used to characterize the MTF. Sensor illumination using the MSTB was performed with both knife-edges and slit. The knife edge, for example, was positioned at the MSTB image plane and illuminated with the edge perpendicular to the spectrometer slit. A steering mirror was tilted so that the image moved across the spectrometer slit in fractional pixel steps for oversampling. These data were used to derive the point spread function and the system MTF (Figure 14 and Table 4). A similar process was conducted with a slit replacing the knife edge.

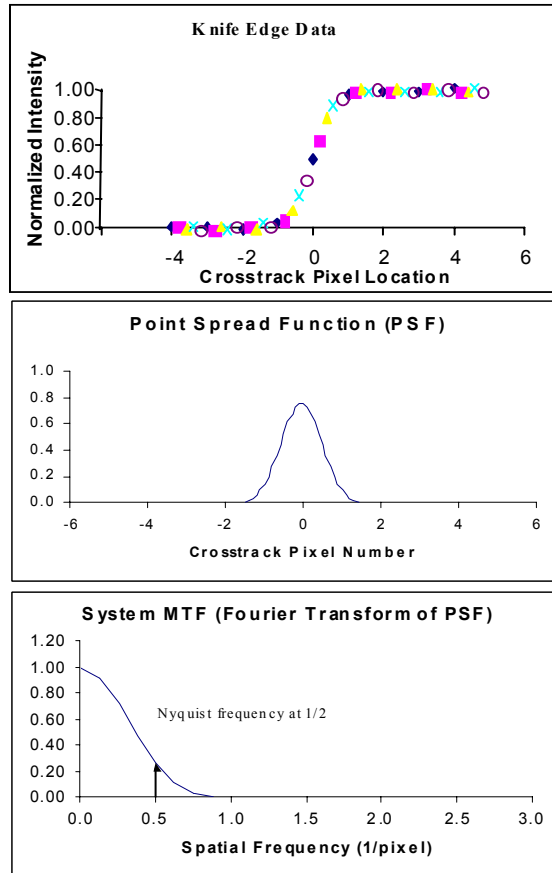


**Figure 14. Knife-edge Measurements and Analysis Provide MTF Characteristics**

**Table 4. MTF Lab Measurement Results Using Knife-edge Technique**

$\lambda$ ( $\mu\text{m}$ )	FOV > 200	Center FOV	FOV < 20
0.5	0.29	0.27	0.22
0.63	0.27	0.28	0.22
0.90	0.24	0.26	0.22
1.05	0.28	0.3	0.28
1.25	0.28	0.3	0.27
1.65	0.27	0.27	0.25
2.2	0.28	0.27	0.23

An innovative approach to the same objective used an image simulator with a starburst pattern (Figure 15). The MTF was determined by examining the image clarity moving into the center of the image. The results were similar to the knife-edge measurements.

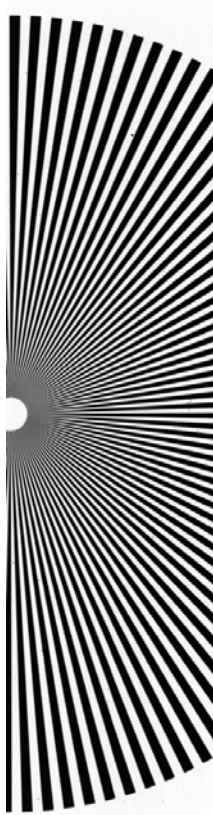


**Figure 15. Two Dimensional Patterns Were Used to Measure MTF**

The on-orbit approach to validating the MTF involved modeling the instrument response to ground targets with sharp edges including bridges, edges of ice shelves and the Moon [24]. Bridge scenes produced excellent correlation with the pre-flight measurements. Several “cross-track” and in-track” bridges were selected for these measurements. Figure 16 shows a Hyperion image acquired on December 24, 2000 of the Mid-Bay Bridge near Eglin AFB in Destin, Florida. To measure the MTF, the Line Spread Function (LSF) was sampled at a higher resolution than the GSD. This was accomplished by analyzing an object at a slight angle to the spacecraft direction and interlacing the consecutive frames. In the bridge scene of Figure 15, the angle between the orbital track and the bridge was too small to use consecutive frames so every fifth frame was used in the interlaced LSF. The interlaced LSF was then processed with a Fourier transform and adjusted by the bridge width to determine the MTF. The results of the analysis and model are shown in Figure 17. The MTF measured at the Nyquist sampling frequency using this scene agreed with the pre-flight measured value of 0.42. Based on the average difference between the pre-flight and on-orbit MTF measurements, there was no change in the Hyperion optical performance due to the launch or operational environment.

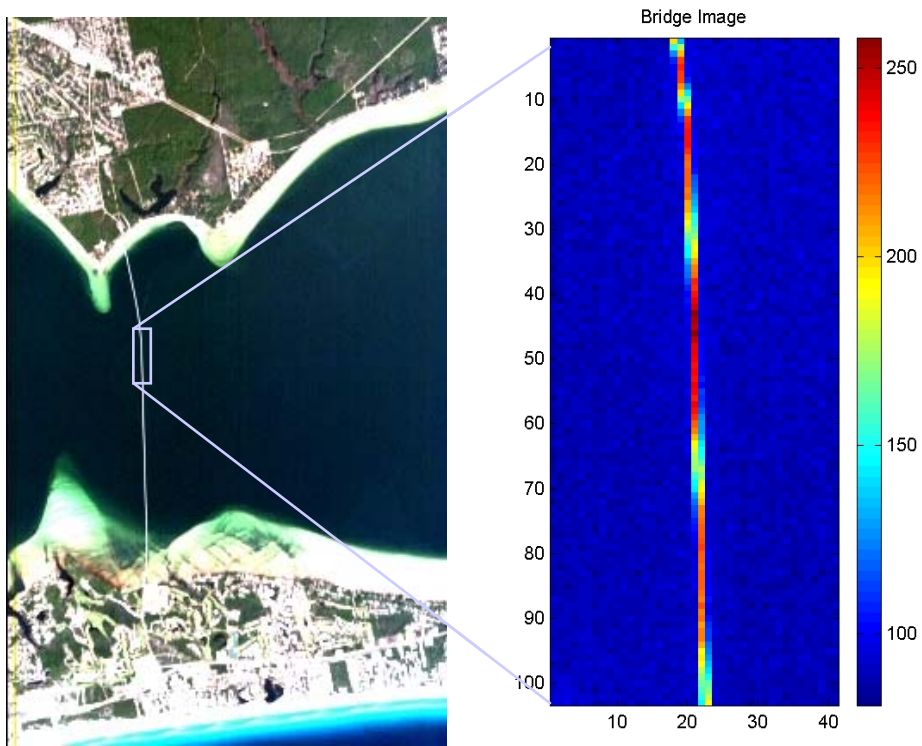


**Figure 16. The Mid-Bay Bridge Near Eglin AFB in Destin, FL, was Used to Measure the MTF**

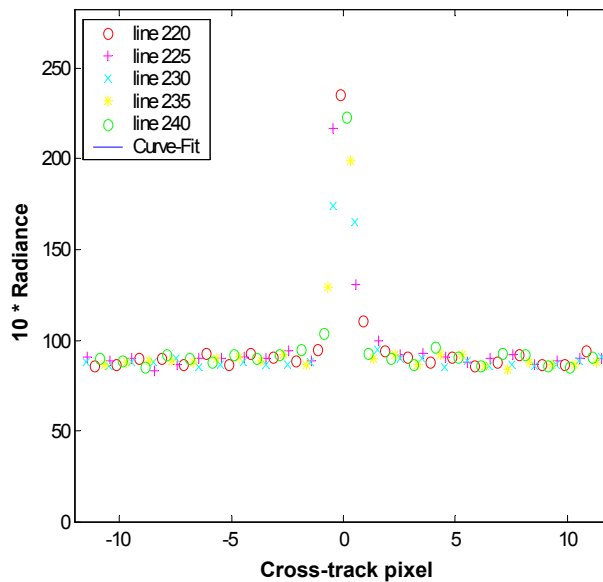


**Figure 17. On-orbit Measurements of MTF Using Interlaced Bridge Images**

Ground Sample Distance

The on-orbit GSD was measured using: (1) a pixel count method between known targets (i.e. known distances) in the images; and (2) a geo-correction process with multiple control points and orthorectified aerial photographs. The pixel count method gave a GSD of 30.4 meters cross-track and 30.4 meters in-track with standard deviations of 0.25m and 0.073m, respectively. The measurements are summarized in Table 5.

**Table 5. Measurement of GSD Over Many Images Show Good Consistency**

<u>Scene</u>	<u>X GSD(m)</u>	<u>Y GSD(m)</u>
Washington DC, Day 356	30.2074	30.7147
New York City, Day 358	30.3856	30.5449
El Segundo, Day 362	30.1425	30.6036
Cape Canaveral, Day 013	30.0234	30.5505
Coleambally, Day 002	30.7310	30.4352
New York City, Day 040 (SWIR)	30.6020	30.5631
El Segundo, Day 362 (SWIR)	30.1303	30.5662
Lake Frome Tarps, Day 5	30.5624	30.5328
Lake Frome Tarps, Day 5 (SWIR)	30.5269	30.5291
Average	30.367	30.560
Standard Deviation (meter)	0.25	0.073

For the second approach, the on-ground pixel size was measured through geo-correcting a set of images using highly accurately surveyed ground points and ortho-rectified aerial images. A detailed study was conducted at a level agricultural site in Coleambally, NSW, Australia [25]. Since the VNIR and SWIR were separate spectrometers, the two data sets were treated as independent images. Three separate Coleambally collections over the January to March 2001 timeframe provided six images that were interactively optimized along with the ground control points and aerial orthophotographs. The resulting GSDs were  $30.77 \text{ m} \pm 0.005 \text{ m}$  in-track and  $30.49 \text{ m} \pm 0.007 \text{ m}$  for cross-track. Also, analyses of the average positional accuracy across the entire Coleambally image had root mean square errors (ranges) of  $12.9 \text{ m} \pm 0.6 \text{ m}$  and  $11.6 \text{ m} \pm 2.1 \text{ m}$ , respectively in the cross- and in-track direction [25]. These results and those above depend to a small extent on the latitude and off nadir pointing position of the scene. For high precision, these numbers must be derived for each site.

### **3.3 Spectral Calibration**

#### **3.3.1 Pre-Launch Spectral Calibration**

Laboratory measurements with the MSTB characterized the spectral shape of 25 pixels distributed systematically in a 5 x 5 array around each of the focal planes. The shape was well represented by a Gaussian profile. The distance between band to band center wavelengths for the VNIR and SWIR dispersions were 10.19 nm/pixel and 10.09 nm/pixel respectively [26]. The results of the spectral calibration measurements performed by a monochromator are shown in Table 6. The band centers and shapes for the remainder of the pixels were derived through interpolation between the measured points. The wavelengths at the band centers are given in Appendix A. A spectral variation across the field of view (termed “smile”) was measured using the laboratory MSTB. The maximum shift was approximately 2.5 nm out of a bandwidth of 10 nm. The VNIR and SWIR spectrometers had different characteristic smiles as shown in Figures 18 and 19. In the figures, the data was normalized to pixel 128 for convenience. The smile in the SWIR was minimal. For the VNIR, the importance of smile – or the

wavelength shift as a function of position in the swath – depended on the application. For example, atmospheric correction codes, which rely on narrow atmospheric lines for their processing, were particularly sensitive to smile. For this correction, it may be necessary to treat each swath position as an “independent” spectrometer for more exacting analysis. This would require more computation, although it would not be technically difficult.

In addition to the monochromator-based measurements, two techniques were used for spectral calibration in the laboratory. The diffuser paint on the back of the HSA cover had a spectral signature in the infrared consisting of three absorption lines at approximately 1190 nm, 1690 nm and 1740 nm (Figure 20). These were also observed on orbit, both during solar and lamp calibrations and were used to verify that the spectral response performance did not change from pre-launch to post-launch.

**Table 6. Hyperion Spectral Calibration Derived from Laboratory Monochromator Measurements**

VNIR Channel Center Wavelengths (nm, accuracy +/- 0.5 nm)					
Spectral channel \ FOV #	13	31	40	48	57
6	477.40	656.46	753.6	834.29	925.38
71	478.45	657.45	754.12	834.91	925.14
136	477.97	656.83	753.66	834.40	925.29
196	476.75	655.69	752.83	833.41	924.38
251	475.15	654.59	751.3	831.94	922.77
SWIR Channel Center Wavelengths (nm +/- 0.5 nm)					
Spectral channel \ FOV #	27	57	87	126	156
6	2314.08	2012.19	1711.16	1314.34	1013.3
71	2314.18	2012.11	1711.42	1315.19	1013.21
136	2313.97	2012.19	1711.55	1315.12	1013.23
196	2313.9	2012.1	1711.62	1315.14	1013.19
251	2313.66		1711.07	1314.22	1012.93
VNIR FWHM of Spectral Response Functions (nm)					
Spectral channel \ FOV #	13	31	40	48	57
6	11.23	10.51	10.6	11.12	11.11
71	11.6	10.38	10.85	11.34	11.34
136	11.34	10.26	10.68	11.26	11.31
196	11.38	10.21	10.69	11.35	11.3
251	11.25	10.16	10.62	11.28	11.23
SWIR FWHM of Spectral Response Function (nm)					
Spectral channel \ FOV #	27	57	87	126	156
6	10.44	10.64	11.55	10.55	10.69
71	10.45	10.79	11.4	10.6	11.01
136	10.42	10.93	11.84	10.83	11.18
196	10.45	11.05	11.59	10.8	11.19
251	10.19		11.33	10.6	11.02

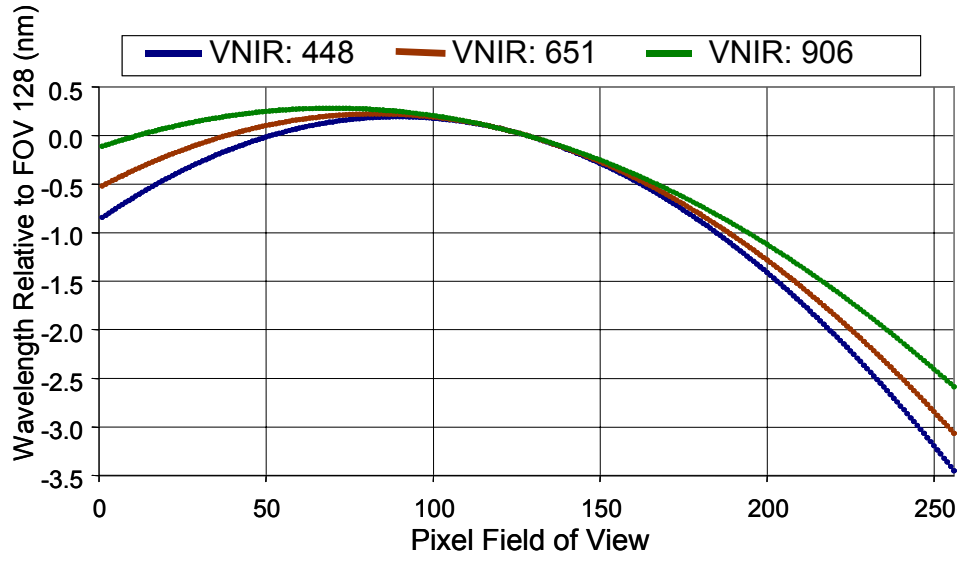


Figure 18. VNIR Spectral Variation Across the Field of View

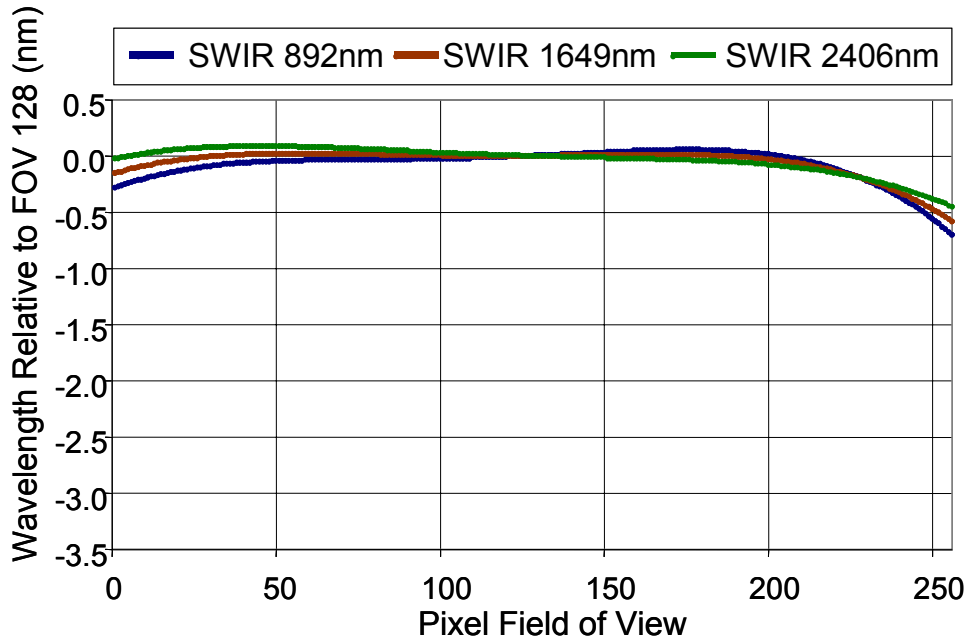
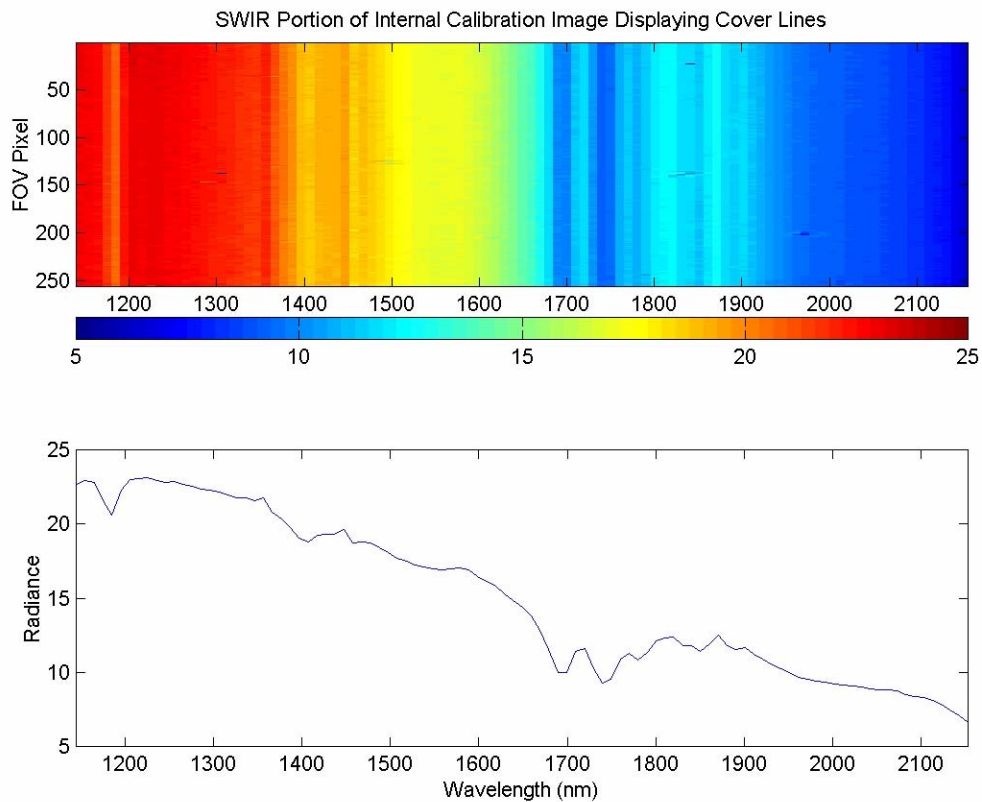


Figure 19. SWIR Spectral Variation Across the Field of View



**Figure 20. SWIR Portion of the Internal Calibration Image Displaying Instrument Cover Paint Spectral Patterns**

The second spectral calibration technique used spectralon doped with either Erbium or Holmium. The light that reflected off of the spectralon had unique spectral absorption lines due to the doping (Figure 21). For the calibration measurements, two images were acquired, one using the doped spectralon and the other taken with the undoped spectralon. The data in the two images were ratioed, which removed both lamp source wavelength and sensor response variations. High-resolution scans of the doped spectralon subsequently convolved with the sensor response agreed extremely well with the other sensor measurements (Figures 22 and 23) [27].

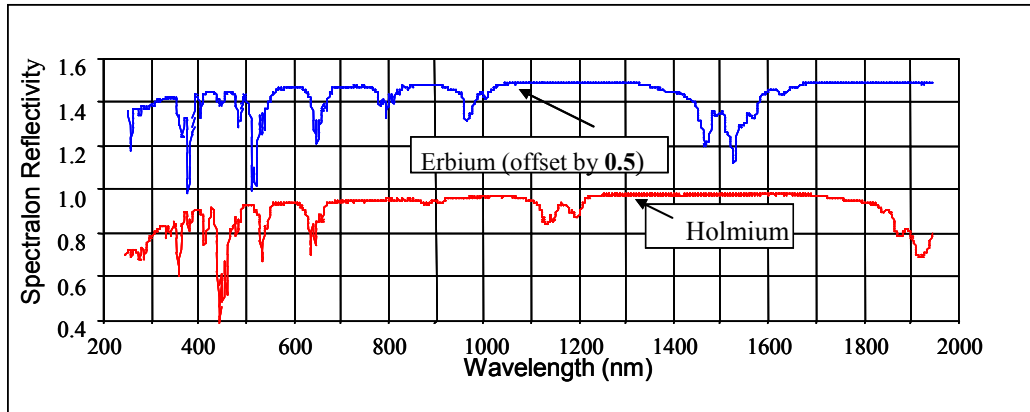


Figure 21. Reflectance Spectra of Doped Spectralon

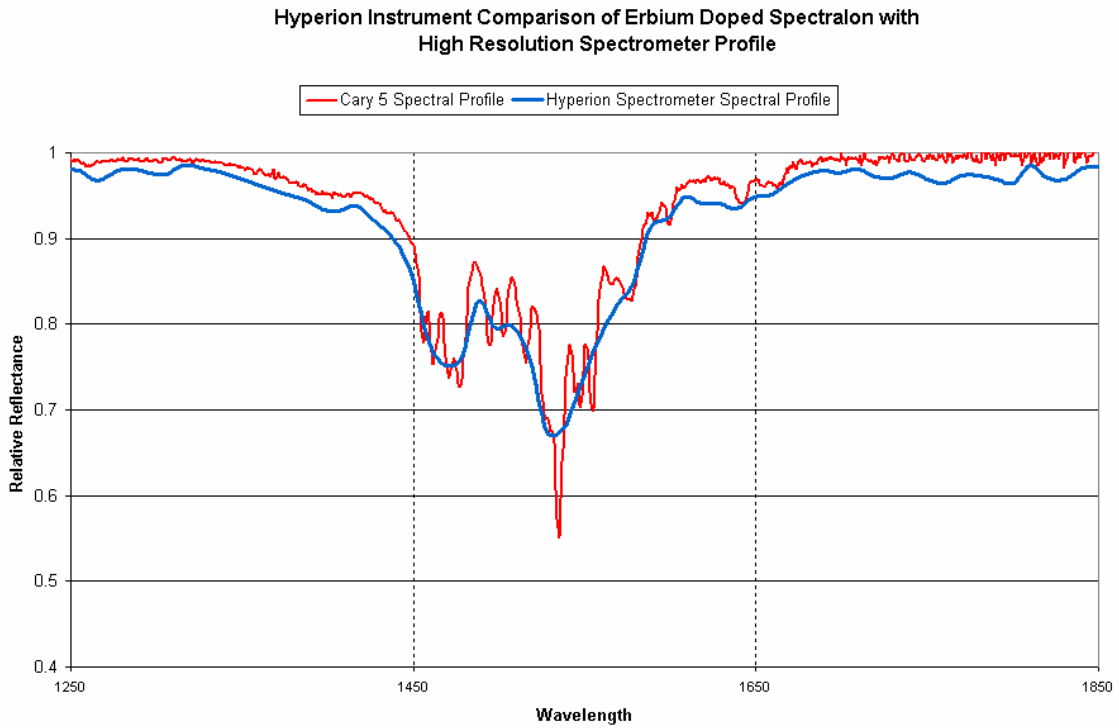
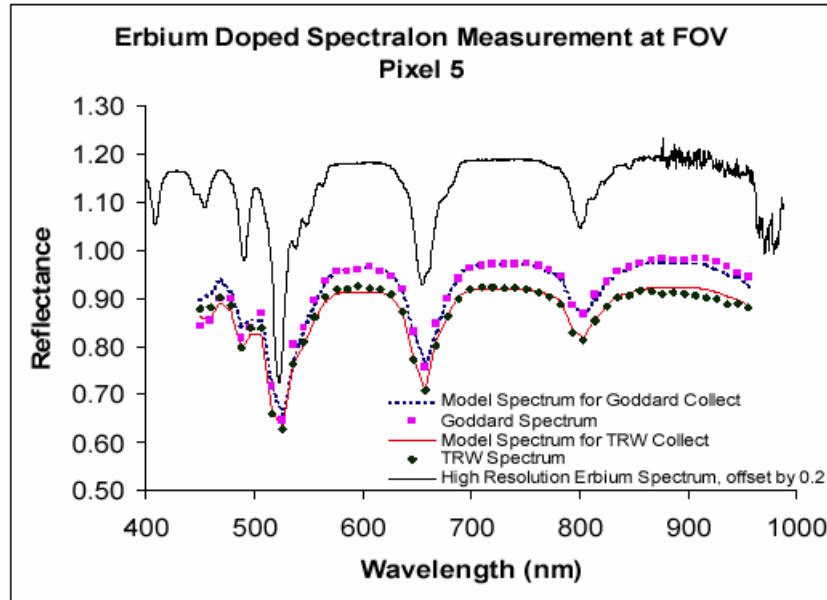


Figure 22. Comparison of High Resolution and Hyperion Measurement of Erbium-doped Spectralon



**Figure 23. Measurement of Hyperion Spectral Response Before (TRW) and After Spacecraft Integration and Environmental Testing (GSFC)**

### 3.3.2 On-Orbit Spectral Calibration

On-orbit spectral verification was more challenging. Spectrally pure ground features of a size to extend across the full swath are extremely rare. One such class of targets was the mineral absorption features above 2000 nanometers. In this spectral range, the signal-to-noise was still sufficient to provide usable signals for analysis. The results of the measurements were consistent with the pre-launch laboratory measurements, but did not provide images with narrow spectral line positions, in part due to signal to noise constraints [28].

Another technique, a data collection of solar radiation transmitted through the earth's atmospheric limb, provided uniform, tractable data for spectral analysis. The atmospheric limb/solar calibration collect viewed the sun through different tangent heights of the atmosphere (see Figures 24 and 25). Because Hyperion viewed the sun scattered off the solar diffuser, the result was a data acquisition that was uniform across the field of view and contained spectral features. These were matched with solar lines, atmospheric lines and absorption lines associated with the solar diffuser (Figure 26). The process enabled the center wavelengths and variations of the center wavelengths across the field of view (i.e., the smile) to be characterized on-orbit for specific wavelengths [26]. For the VNIR, the band center wavelength variability was from 1.7 nm to 2.55 nm, measured on-orbit. This is a shift of about 1 nm from the pre-launch measurements, as shown in Figure 27. The SWIR had minimal smile effect. Maps of the shifts across the focal plane are given in Figure 28. Some uncertainties remain in the spectral location of features associated with the atmosphere and the validity of interpolating between the measured wavelengths. The magnitude of this effect for the VNIR and SWIR is still being studied using the Oxygen, Carbon Dioxide and other spectral signatures [29].

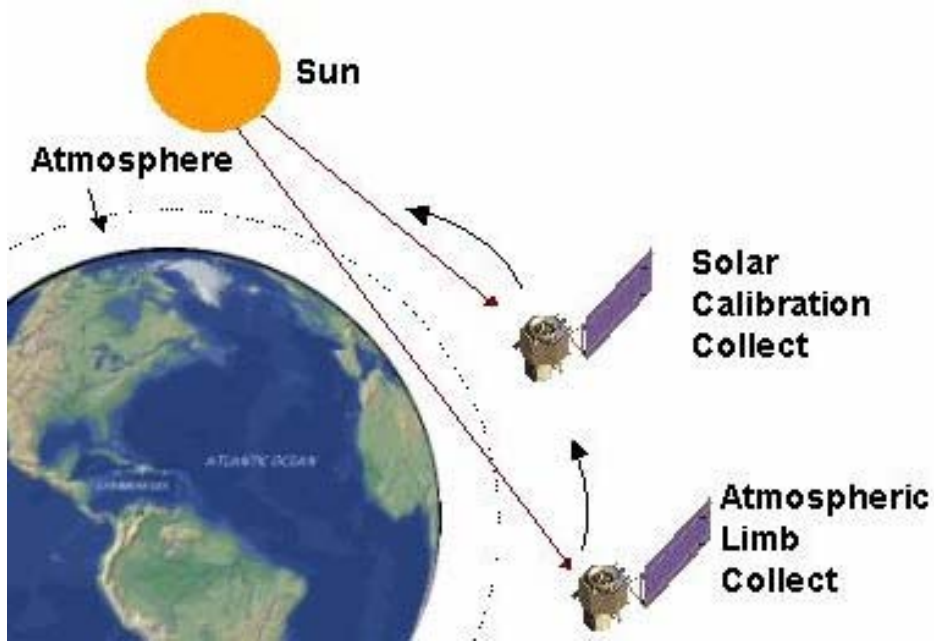


Figure 24. Atmospheric Limb Measurements Enable Spectral Measurement Without Earth Background

Atmospheric Limb Data at Various Times During the Collect

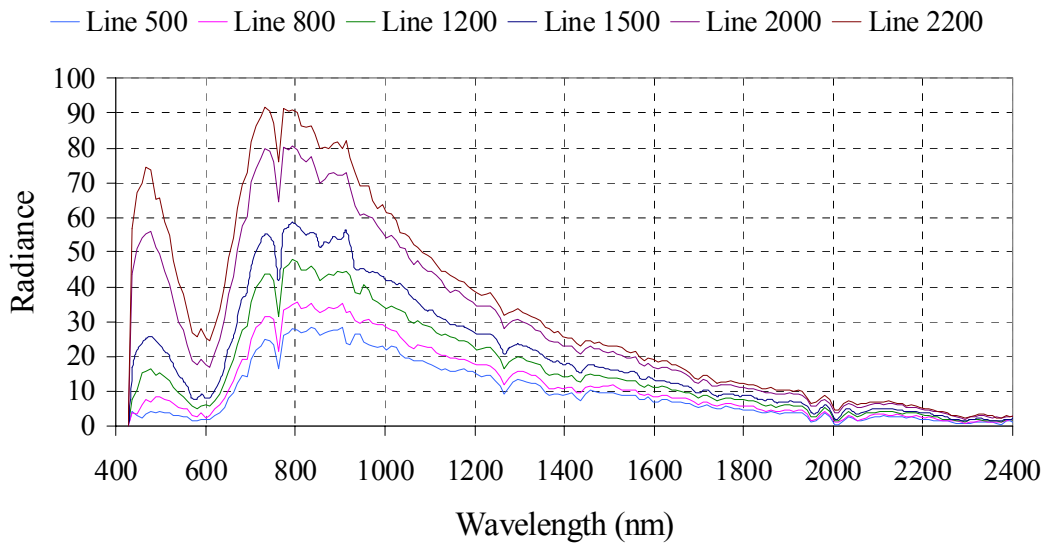
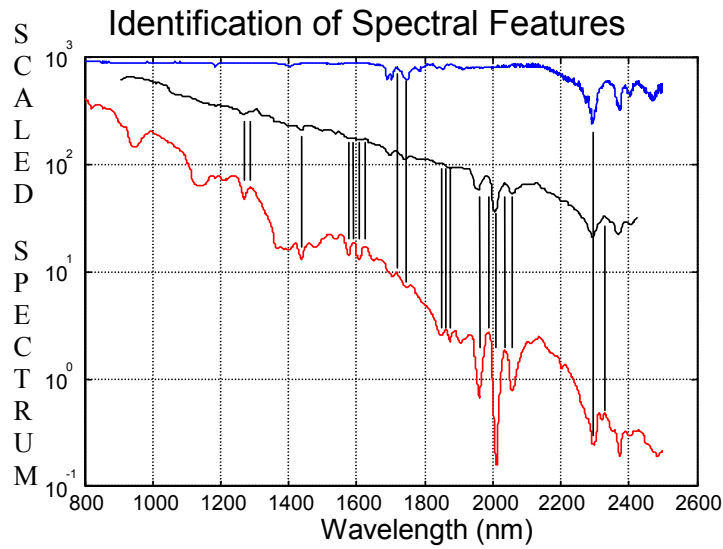
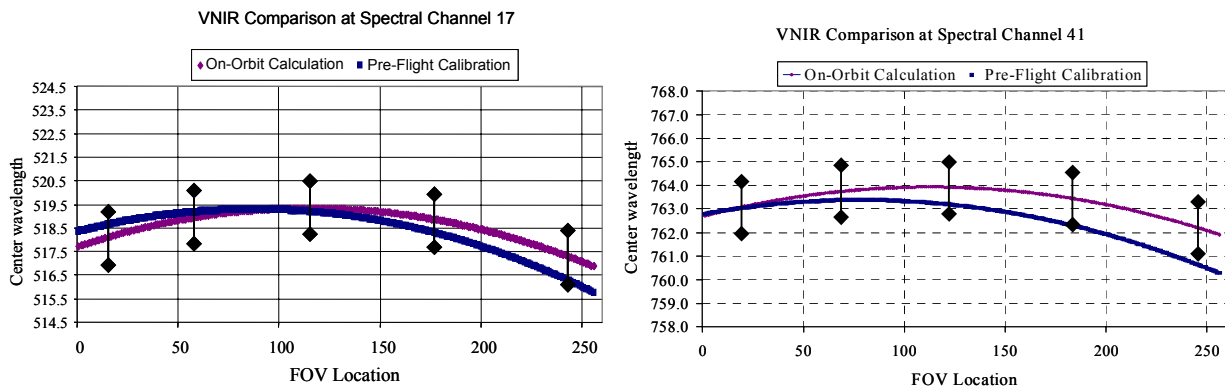


Figure 25. Six Spectral Profiles of the Atmospheric Limb, Measured at Different Grazing Positions



**Figure 26. Analysis of Atmospheric Limb Measurement Showing: Hyperion Spectra of Atmospheric Limb Collect (red); Measured Diffuse Cover Reflectance (blue); and Atmospheric Reference Profile from Modtran 3 (black)**



**Figure 27. Comparison of Laboratory and On-orbit Smile Characteristics for Spectral Channels 17 and 41**

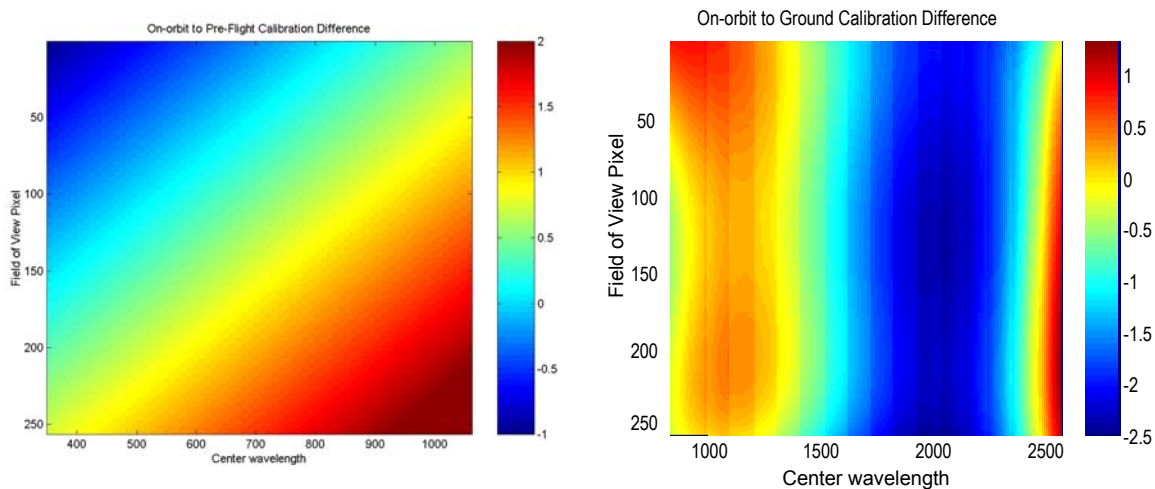


**Figure 28. Differences in Laboratory and On-orbit Spectral Calibrations for the VNIR (left) and SWIR (right) Spectrometers**

### 3.4 Polarization

There was some concern that applications for targets with polarized reflections would be impacted if Hyperion had a strong polarization effect. Thus, the polarization sensitivity was measured in the laboratory. The measurement used dual polarizers that were rotated to map the polarization characteristics. Results for the VNIR and SWIR are shown in Figure 29. The variability was about five percent about the mean response. This was deemed acceptable by the EO-1 Mission Scientist. Polarization response measurements were not performed on-orbit.

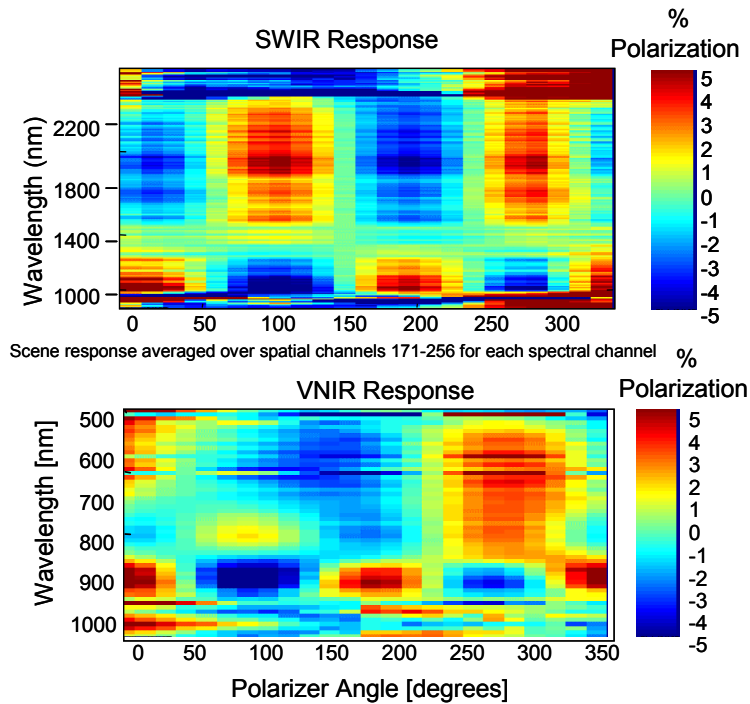


**Figure 29. VNIR and SWIR Polarization Characteristics**

#### **4. IMAGE AND DATA PROCESSING**

The EO-1 spacecraft was in a sun-synchronous orbit with an altitude of 705 km, a 10:01 AM descending node and a 16 day repeat cycle. The spacecraft was capable of a 22 degree or more roll angle and data were acquired with the spacecraft rolled to various pointing angles. The angle was held constant during an image acquisition. Typical pointing accuracies at the Earth’s surface were 100 m cross-track and the associated pointing knowledge was 40 m cross-track and 100 m along track. A DCE included the scene image, dark images and the ancillary data needed for image processing. For Hyperion, a typical image cube consisted of approximately 6000 frames of data and required about 27 seconds to collect. Data collections up to two minutes were possible, limited by the solid-state memory.

During the first year of operations, the Level 1 radiometric processing was done at TRW on Level 0 data provided by EO-1 operations at Goddard Space Flight Center. Level 1 processing provided a number of correction and calibration functions. Initially, it used the preflight calibration developed during environmental testing for pixel gains and identified bad pixels whose values were replaced by nearest neighbor averages. The offset for each pixel derived from the cover closed “dark” image was subtracted during the Level 1 processing. Corrections for smear and echo, discussed above, were also included. Level 1 processing output was in a computer compatible format for further processing and analysis.

During the first year of operations, the Level 1 data processing evolved as further experience was gained with the instrument (Table 7). A major change in processing and data format was implemented seven months after launch. The data format was modified from an unsigned to a signed integer to include both positive and “negative” data, allowing for noise fluctuations around zero. The offset calculation was changed from nearest dark collect to a linear interpolation between dark collects before and after image

collection. This was done because a small drift in dark level was observed over the several minutes of a data collection sequence, as shown in Figure 30. Also, a saturated pixel report was created. Saturation in the SWIR was observed when imaging very bright thermal sources such as volcanic eruptions or intense fires. Since the echo correction was defined as a known percentage of the related pixel intensity, saturation caused errors in the echo correction. The echo correction for saturation pixels was eliminated. Sample spectra of data processed through Level 1 are shown in Figure 31. These spectra, derived from a Coleambally image, are not corrected for atmospheric effects.

**Table 7. Evolution of Level 1 Processing**

Level 1 version	.cal	.L1	.L1_A	.L1_A3	.L1_B
Effective date	pre-flight	4/1/2001	7/1/2001	10/23/2001	11/15/2001
<b>Level 1 parameters mods</b>					
Ratio file	ratio.txt	ratio.txt	ratio_revA.txt	ratio_revB.txt	ratio_revB.txt
Gain file	PriRadL0.bin	hypgain.txt	HypGain_revA.dat	HypGain_revB.dat	HypGain_revB.dat
Data type	uint16	uint16	int16	int16	int16
Calibration multiplier VNIR	100	100	40	40	40
Calibration multiplier SWIR	100	100	80	80	80
Cal Min	0	0	-32768	-32768	-32768
Cal Max		40000	32768	32767	32767
Bad pixel file	badpix	badpix2	badpix2	badpix3	badpix3
<b>Level 1 algorithm mods</b>					
Bad pixel repair	yes	yes	yes	yes	yes
Saturated pixel report	no	no	yes	yes	yes
Offset removal	nearest	nearest	interpolated	interpolated	interpolated
VNIR/SWIR co-alignment	no	no	no	no	yes

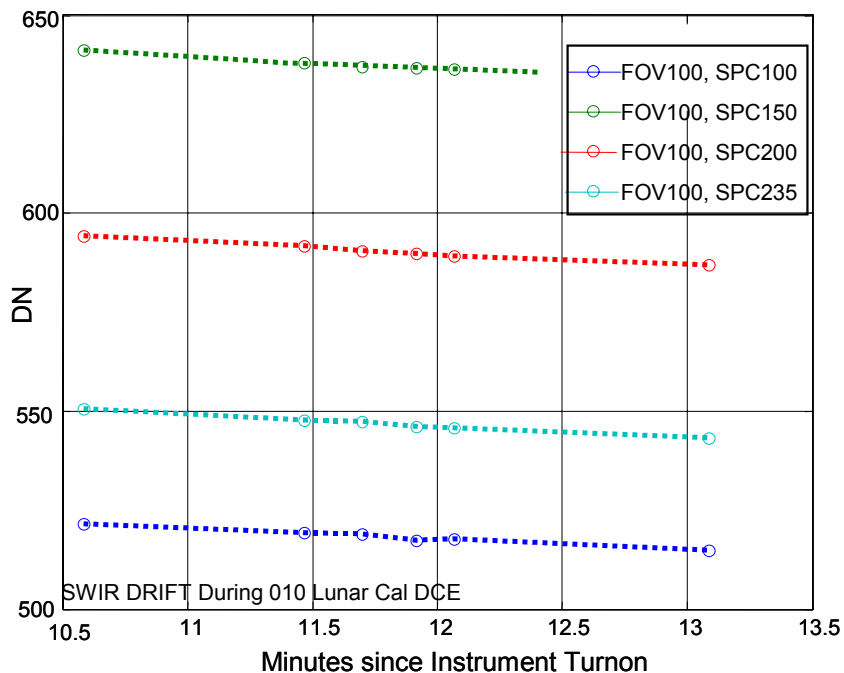


**Figure 30. Dark Signal Drift as a Function of Time During a Data Collection Sequence**

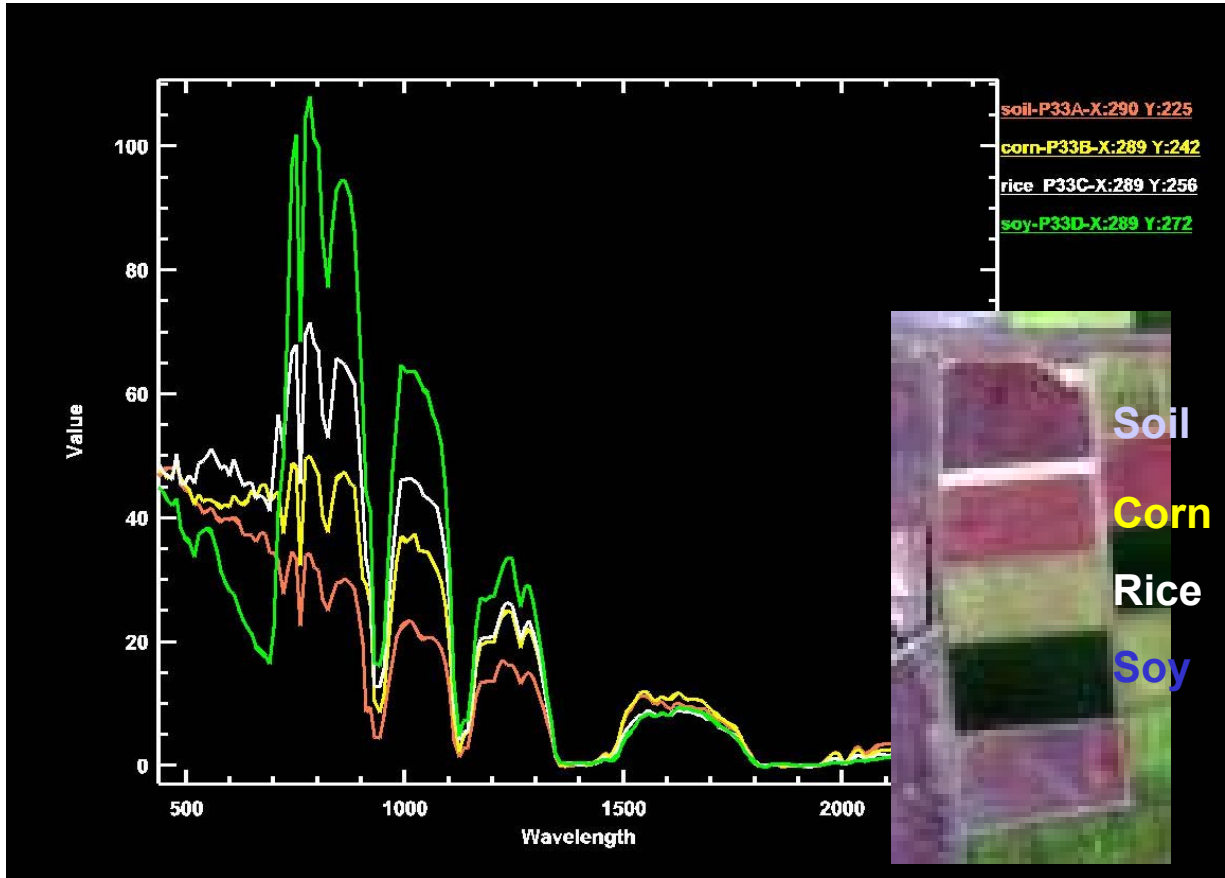


**Figure 31. Sample Spectra From Level 1 Processing**

By one year after launch, sufficient vicarious, lunar and solar collects had been analyzed to create final gain coefficients for each pixel. As previously noted, these were typically 8% greater for the VNIR and 18% greater for the SWIR than the pre-launch values. These changes were not due to a change in instrument characteristics, but represented an update of the laboratory calibrations factors to provide better correlation between Hyperion and Landsat 7. The new gain coefficients were used on all data processed after calendar year 2000. Starting in February 2001, USGS EROS Data Center (USGS EDC) assumed responsibility for routine data processing.

In addition to the above factors, Level 1B1 processing performed an alignment of the VNIR and SWIR spectrometer images to within approximately half a pixel. There was a known one pixel shift between the VNIR and SWIR images in the cross-track direction. The in-track direction was more complex because the shift varied linearly across the swath. This was due to the differences in readout techniques for the two focal planes: the VNIR focal plane was read out in quadrants while the SWIR focal plane had four readout ports which read adjacent pixels in 2x2 arrays. The result of the different readout processes was that there was a timing difference between the two focal planes so that the VNIR and SWIR images were aligned spatially on the right side of the image (west side for descending orbits) and the SWIR was one in-track pixel later on the left side. The Level 1B1 processing adjusted for this by shifting the SWIR one cross-track pixel and, for the left half of the image, also shifting the SWIR forward one pixel. While not precise, this adjustment was selected because it did not require resampling and was thus reversible. More precise shifts may be performed by the user, if desired.

Experience showed that the Level 1 data had vertical (in-track) striping [30]. Various techniques were used to minimize this striping. This was important for applications that cover more than a small portion of the swath. However, it was a complex issue with imaging spectrometers, which had to consider both spatial and spectral characteristics of the data. Two approaches for stripe removal involved taking the mean and variance of columns along-track for a sufficiently long collect, typically 600-1000 frames. The mean and variance of each column were then set equal to the mean and variance for the entire image. This technique worked well for images of terrain with a random mixture of features such as desert scenes [28]. However, using this approach over large agricultural fields caused the de-striping to alter the spectral characteristics within the image. An alternative approach involving a more local rather than a global mean and variance was reported to avoid the problem of spectral contamination while still removing the striping [31].

The removal of smile was addressed by using a minimum noise function (MNF) transform approach. The dominant part of the smile variability shows up in the first MNF transform. By eliminating the first MNF and using the rest that are significant for applications may facilitate large swath applications research. This technique was used, for example, for Hyperion-based forest species classification [32]. There is still ongoing work to address the smile, as indicated earlier. No single process has been adopted uniformly by the SVT or the Science Community at large.

## 5. LESSONS LEARNED

- Solar and lunar observations were very important for evaluating long-term stability and performance trends. Both capabilities should be built into future systems.
- Laboratory calibration is critical for identifying key system characteristics. Laboratory measurements should not be short changed in the race to launch.
- Creative solutions to on-orbit spectral calibration had to be developed because the pushbroom system did not have a simple option of calibrating on-board in the manner of scanning systems. These were successful as noted in this report.
- The Science Validation Team (SVT) was invaluable in providing feedback to the instrument team. Provisions in future programs should include sufficient resources for in-depth interactions with users (including science teams), particularly for a new instrument technology. Each of the application areas stressed the data in different ways. The breadth of applications was a very positive attribute of the SVT.

## 6. CONTACT INFORMATION

Jay S. Pearlman  
Phantom Works  
The Boeing Company  
Kent, WA 98032  
253-773-2784  
[jay.pearlman@boeing.com](mailto:jay.pearlman@boeing.com)

## 7. SUMMARY

Hyperion was a major advance in space-based hyperspectral instruments. It was designed as a technology demonstration to build and maintain a “science” grade instrument for validating pushbroom performance and to initiate hyperspectral applications on a global scale. While the instrument was built in less than one year, the design goal of a stable, carefully calibrated instrument was achieved.

Hyperion’s 242 bands covered the visible, near infrared and short wave infrared bands (400-2500 nm) with 10 nm bandwidths; typically 198 bands were provided in the calibrated data. The spatial resolution of 30 m was sufficient to address most land cover issues. The pointing and data storage capabilities of the spacecraft allowed global access. The radiometric and spectral performance permitted quantitative temporal hyperspectral monitoring of Earth surface processes, something that had never been done routinely on a global scale.

The advances made through the EO-1 program include the on-orbit operation and performance a pushbroom imaging spectrometer. Many questions had been raised about the ability to predict performance and also to have a design that was stable enough to provide long-term observational capability with the large number of pixels in a pushbroom system. Hyperion answered these questions affirmatively.

The interest in EO-1 has continued and the mission has been extended beyond the original one year. The Hyperion instrument operates without degradation and is providing opportunities for new and expanded research and applications.

## 8. REFERENCES

[1] Ungar, Stephen, J. S Pearlman, J.A. Mendenhall, Dennis Reuter, “Overview of the Earth Observing One (EO-1) Mission,” *Transactions of Geoscience and Remote Sensing (TGRS)*, June 2003 (in publication).

[2] The optical structure was designed, fabricated, and assembled by SSG, Inc., the SWIR focal plane array was produced by Boeing, the VNIR focal plane array was built by Loral, and the gratings were fabricated by JPL.

[3] Ungar, S, “Overview of EO-1, The First 120 Days”, *IEEE International Geoscience and Remote Sensing Symposium*, 1, 43-45, July 9-13, 2001.

[4] Pearlman, J., S. Carman, C. Segal, P. Jarecke, P. Barry and W. Browne, “Overview of the Hyperion imaging spectrometer for the NASA EO-1 mission” *IEEE International Geoscience and Remote Sensing Symposium*, 6, pp 3504-3506, 2001.

[5] Chan, C. K., P. S. Clancy, J. Godden, “Pulse Tube Cooler for Flight Hyperspectral Imaging,” *Cryogenics*, 39, pp. 1007-1014, 1999.

[6] Mourouis, P., D. W. Wilson, P. D. Maker, and R. A. Muller, “Convex Grating for Concentric Imaging Spectrometer,” *Applied Optics*, 37, pp. 7200-7208, 1998.

[7] P. Jarecke, K. Yokoyama, “Radiometric Calibration of the Hyperion Imaging Spectrometer Instrument From Primary Standards to End-to-End Calibration””, *Proc. of SPIE*, 4135, pp.254-263, August 2000.

- [8] Pearlman, J. S, S. Carman, P. Lee, L. Liao, and C. Segal, "Hyperion Imaging Spectrometer on the New Millennium Program Earth Orbiter-1 System," *The 1999 International Symposium on Spectral Sensing Research (ISSSR99) and International Society for Photogrammetry and Remote Sensing (ISPRS) Commission 7, Working Group I: Fundamental Physics and Modeling*, October 31, 1999 - November 4, 1999, Tropicana Resort and Casino, Las Vegas, NV.
- [9] Markham, B. L., J. S. Schafer, F. M. Wood, Jr., P. W. Dabney and J. L. Barker, "Monitoring Large Aperture Spherical Integrating Sources with a Portable Radiometer during Satellite Instrument Calibration," *Metrologia*, 35, #4, 1998, pp. 643-648.
- [10] Jarecke, P., K. Yokoyama, P.S. Barry, "On-Orbit Solar Radiometric Calibration of the Hyperion Instrument" *Proc. of SPIE*, Vol 4480, pp.225-230, 2002.
- [11] Kieffer, H.H., P. Jarecke, J. Pearlman, "Initial Lunar Calibration Observations by the EO-1 Hyperion Imaging Spectrometer," *Proc. SPIE*, 4480, pp 247-258, 2002.
- [12] (a) Kieffer, H.H. and R. L. Widley, "Establishing the Moon as a Spectral Radiance Standard," *Journal of Atmosphere and Oceanic Technology*, 13, 2 pp 360-375, 1996; (b) T.C. Stone and H.H. Kieffer, "Absolute Irradiance of the Moon for On-orbit Calibration," *Proc. SPIE*, 4814, pp. 211-221, 2002.
- [13] Stone, T.C., H.H. Kieffer, "Absolute Irradiance of the Moon for On-orbit Calibration," *Proc. SPIE*, 4814, pp211-221, 2002.
- [14] Kieffer, H.H, Anderson, J.A. and K. J. Becker, "Radiometric Calibration of spacecraft using small lunar images", *Proc. SPIE*, 3870, 193-205, 1999.
- [15] Anderson, J.M., H.H. Kieffer and K.J. Becker, " Modeling the brightness of the Moon over 350-2500 nm for spacecraft calibrations," *Proc SPIE*, 4169, pp 248-259, 2000.
- [16] Kieffer, H.H., T.C. Stone, R.A. Barnes, S. Bender, R. E. Eplee Jr., J. Mendenhall and L. Ong, On-orbit Radiometric Calibration over time and Between Spacecraft," *Proc. SPIE*, 4481, (Crete conference) , 2002.
- [17] Jarecke, P., K. Yokoyama, P.S. Barry, "On-orbit Solar Radiometric Calibration of the Hyperion Instrument," *Proc. SPIE*, 4480, pp.225-230, 2002.
- [18] Jarecke, P.J., P.S. Barry, J.S Pearlman, and B. L. Markham, "Aggregation of Hyperion Hypespectral spectral bands into Landsat-7 ETM+ spectral bands," *Proc. SPIE*, 4480, pp.259-263, 2002.
- [19] Barry, P.S., P. Jarecke, J. Pearlman, D.L.B. Jupp, J. Lovell, S. Campbell, "Radiometric Calibration Validation of the Hyperion Instrument using Ground Truth at a Site in Lake Frome," *Proc. SPIE*, 4480, pp. 242-246, 2002.
- [20] Green, R.O., B.E. Pavri and T. G. Chrien, "On-orbit Radiometric and Spectral Calibration of EO-1 Hyperion Derived with an Underflight of AVIRIS and In Situ Measurements at Sala de Arizaro, Argentina," *TGRS*, June 2003. (in publication).
- [21] Biggar, S, K.J. Thome and W.T. Wisniewski, "Vicarious Radiometric Calibration of EO-1 Sensors by Reference to High Reflectance Ground Targets," *TGRS*, June 2003. (in publication).

- [22] Bindschadler, R, H. Choi, “Characterizing and Correcting Hyperion Detectors using Ice-Sheet Images,” *TGRS*, June 2003. (in publication).
- [23] Dr. Lawrence Ong, private communication.
- [24] Nelson, N., P.S. Barry, ”Measurement of Hyperion MTF from On-Orbit scenes,” *The International Symposium on Optical Science and Technology*, July 29 – August 3, 2001.
- [25] McVicar, T.R., Van Niel, T.G. and Jupp, D.L.B. (2001). Geometric Validation of Hyperion Data acquired by Earth Observing 1 Satellite at Coleambally Irrigation Area. CSIRO Land and Water Technical Report 46/01.
- [26] Barry, P.S., J. Shepanski, C. Segal, “Hyperion On-Orbit Validation of Spectral Calibration using Atmospheric Lines and On-Board System,” *The International Symposium on Optical Science and Technology*, July 29 – August 3, 2001.
- [27] Liao, L, P. Jarecke, D. Gleichauf, T. Hedman, “Performance Characterization of the Hyperion Imaging Spectrometer Instrument,” *Proc. SPIE*, 4135, 264-275, 2000.
- [28] Cudahy, T.J.; Rodger, A.P.; Barry, P.S.; Mason, P.; Quigley, M.; Folkman, M.; Pearlman, J., “Assessment of the stability of the hyperion SWIR module for hyperspectral mineral mapping using multi-date images from Mount Fitton, Australia” *IEEE International Geoscience and Remote Sensing Symposium*, 6, pp. 3504 –3506, 2002.
- [29] Private communications from DLB Jupp(CSIRO), R. Green(JPL) and B Carlson(NASA GIS).
- [30] Han, T, *IEEE International Geoscience and Remote Sensing Symposium*, 6, pp. 3504 –3506, 2002.
- [31] Datt B., T.R. McVicar, T.G. Van Niel, D.L. Jupp, J.S Pearlman, “Pre-processing EO-1 Hyperion Hyperspectral Data to Support the Application of Agricultural Indices,” *TGRS*, June 2003. (in publication).
- [32] Goodenough, D.G., A. Dyke, K.O. Niemann, J.S Pearlman, A.S. Bhogal, T. Han, M. Murdoch, C. West, “Monitoring Forests with Hyperion and ALI,” *TGRS*, June 2003 (in publication).

## APPENDIX A – HYPERION WAVELENGTHS

BAND #	WAVE-LENGTH								
1	355.6	51	864.4	101	1154.6	151	1659.0	201	2163.4
2	365.8	52	874.5	102	1164.7	152	1669.1	202	2173.5
3	375.9	53	884.7	103	1174.8	153	1679.2	203	2183.6
4	386.1	54	894.9	104	1184.9	154	1689.3	204	2193.7
5	396.3	55	905.1	105	1195.0	155	1699.4	205	2203.8
6	406.5	56	915.2	106	1205.1	156	1709.5	206	2213.9
7	416.6	57	925.4	107	1215.2	157	1719.6	207	2224.0
8	426.8	58	935.6	108	1225.2	158	1729.7	208	2234.1
9	437.0	59	945.8	109	1235.3	159	1739.7	209	2244.2
10	447.2	60	955.9	110	1245.4	160	1749.8	210	2254.2
11	457.3	61	966.1	111	1255.5	161	1759.9	211	2264.3
12	467.5	62	976.3	112	1265.6	162	1770.0	212	2274.4
13	477.7	63	986.5	113	1275.7	163	1780.1	213	2284.5
14	487.9	64	996.6	114	1285.8	164	1790.2	214	2294.6
15	498.0	65	1006.8	115	1295.9	165	1800.3	215	2304.7
16	508.2	66	1017.0	116	1306.0	166	1810.4	216	2314.8
17	518.4	67	1027.2	117	1316.1	167	1820.5	217	2324.9
18	528.6	68	1037.3	118	1326.1	168	1830.6	218	2335.0
19	538.7	69	1047.5	119	1336.2	169	1840.6	219	2345.1
20	548.9	70	1057.7	120	1346.3	170	1850.7	220	2355.2
21	559.1	71	851.9	121	1356.4	171	1860.8	221	2365.2
22	569.3	72	862.0	122	1366.5	172	1870.9	222	2375.3
23	579.4	73	872.1	123	1376.6	173	1881.0	223	2385.4
24	589.6	74	882.2	124	1386.7	174	1891.1	224	2395.5
25	599.8	75	892.3	125	1396.7	175	1901.2	225	2405.6
26	610.0	76	902.4	126	1406.8	176	1911.3	226	2415.7
27	620.1	77	912.5	127	1416.9	177	1921.4	227	2425.8
28	630.3	78	922.5	128	1426.9	178	1931.5	228	2435.9
29	640.5	79	932.6	129	1437.0	179	1941.6	229	2446.0
30	650.7	80	942.7	130	1447.1	180	1951.6	230	2456.1
31	660.8	81	952.8	131	1457.2	181	1961.7	231	2466.1
32	671.0	82	962.9	132	1467.3	182	1971.8	232	2476.2
33	681.2	83	973.0	133	1477.4	183	1981.9	233	2486.3
34	691.4	84	983.1	134	1487.5	184	1992.0	234	2496.4
35	701.5	85	993.2	135	1497.6	185	2002.1	235	2506.5
36	711.7	86	1003.3	136	1507.7	186	2012.2	236	2516.6
37	721.9	87	1013.3	137	1517.8	187	2022.3	237	2526.7
38	732.1	88	1023.4	138	1527.9	188	2032.4	238	2536.8
39	742.3	89	1033.5	139	1537.9	189	2042.5	239	2546.9
40	752.4	90	1043.6	140	1548.0	190	2052.5	240	2557.0
41	762.6	91	1053.7	141	1558.1	191	2062.6	241	2567.0
42	772.8	92	1063.8	142	1568.2	192	2072.7	242	2577.1
43	783.0	93	1073.9	143	1578.3	193	2082.8		
44	793.1	94	1084.0	144	1588.4	194	2092.8		
45	803.3	95	1094.1	145	1598.5	195	2102.9		
46	813.5	96	1104.2	146	1608.6	196	2113.0		
47	823.7	97	1114.2	147	1618.7	197	2123.1		
48	833.8	98	1124.3	148	1628.8	198	2133.2		
49	844.0	99	1134.4	149	1638.8	199	2143.3		
50	854.2	100	1144.5	150	1648.9	200	2153.3		